TECHNISCHE UNIVERSITÄT WIEN

Master Thesis

Mg – substituted Lithium Vanadium Phosphate (LVP) as an electrode material for Lithium Ion Batteries (LIB)

Technische Universität Wien
Institute of Chemical Technologies and Analytics
Getreidemarkt 9/164-CT
1060 Wien

Under the supervision of Ao. Univ. Prof. Dipl.-Ing. Dr.techn. Günter Fafilek

Fabian Bohrn, BSc
Franz-Josefs Kai 23/16
1010 Wien

Ich habe zur Kenntnis genommen, dass ich zur Drucklegung meiner Arbeit unter der Bezeichnung

Masterarbeit

nur mit Bewilligung der Prüfungskommission berechtigt bin.

Ich erkläre Eides statt, dass ich meine Masterarbeit nach den anerkannten Grundsätzen für wissenschaftliche Abhandlungen selbstständig ausgeführt habe und alle verwendeten Hilfsmittel, insbesondere die zugrunde gelegte Literatur, genannt habe.

Weiters erkläre ich, dass ich dieses Masterarbeitsthema bisher weder im In- noch Ausland (einer Beurteilerin/einem Beurteiler zur Begutachtung) in irgendeiner Form als Prüfungsarbeit vorgelegt habe und dass diese Arbeit mit der vom Begutachter beurteilten Arbeit übereinstimmt.

Wien, am 8. Oktober 2018

_____

Fabian Bohrn, BSc

Danksagung

Der größte Dank gilt meiner Familie, die mir den sich seit dem Gymnasium gefestigten Traum Chemie zu studieren ermöglicht hat. Das mit Obst und Kaffee beim Lernen für Prüfungen versorgen, das Zuhören, wenn ich über richtungsweisende Entscheidungen nachgedacht habe, das Motivieren, wenn manche Prüfungen nicht auf Anhieb klappten und respektieren, wenn ich Entscheidungen getroffen habe.

An meine Freunde, die mir gut zugeredet haben, während dieser Arbeit und meine StudienkollegInnen mit denen ich in allen Labors und beim Lernen viel Spaß hatte. An meine BetreuerInnen und ProfessorInnen die meinen Wissensdurst gestillt und meine teilweise komplexen Fragen beantwortet haben.

Besonderer Dank gilt dem AIT, dass mir die Durchführung der Arbeit ermöglichte und mir eine breite Wissenspalette und Austauschfläche bot, aus welcher ich schöpfen konnte und die sehr gründliche, persönliche Betreuung von dir, Arlavinda.

Danke an die Forschungsgruppe von Prof. Limbeck an der TU Wien für die Ermöglichung der ICP-OES Messungen und an die Forschungsgruppe von Prof. Sedlarikova am FEKT in Brno, CZ für die ergänzenden Methoden und Einblicke in die Arbeitsweisen der Elektrochemie in anderen Ländern.

Zusammenfassung

Der weltweite Energiebedarf steigt laufend. Immer lauter wird der Ruf nach Bereitstellung dieser Energie aus nachhaltigen, erneuerbaren Quellen, wie Luft, Wasser und Sonne. Diese Quellen haben den Nachteil, dass die Produktion Umwelteinflüssen wie Tages- und Jahreszeit, Niederschlag usw. unterliegt. Dadurch steigt die Bedeutung von Speicherstätten für Energie. Die leichtest speicherbare und wandelbarste Form der Energie ist elektrische Energie. Eine mögliche Speicherstätte dafür sind Lithiumionenbatterien, deren Kapazität unter anderem von den verwendeten Elektrodenmaterialien abhängt. Daher wird sehr viel Forschung im Bereich der Elektrodenmaterialien betrieben.

Lithiumvanadiumphosphat ($Li_3V_2(PO_4)_3$) ist ein Elektrodenmaterial, welches sowohl als Kathode als auch Anode eingesetzt werden kann. Bei der Anwendung als Kathodenmaterial zeigt es den unerwünschten Effekt, des schnellen Kapazitätsverlusts durch wiederholte, strukturelle Veränderung bei fortschreitender Zahl der Lade-Entladezyklen. Der in dieser Arbeit untersuchte Ansatz der Strukturstabilisierung beruht auf dem Prinzip der teilweisen Substitution von Vanadium (V^{3+}) durch Magnesium (Mg^{2+}), welches einen fast identen Ionenradius aufweist und daher auf atomarer Ebene bei der Stabilisierung der Gitterparameter dienen soll.

Es wurde Lithiumvanadiumphosphat ohne, sowie mit unterschiedlichen Substitutionskonzentrationen an Magnesium im Bereich von (0,016 bis 0,053) synthetisiert und charakterisiert. Dabei wurden sowohl physikochemische Eigenschaften, welche mittels TG-DSC, ICP-OES, Cilas, XRD und BET ermittelt wurden und elektrochemische Eigenschaften welche mit CV, GC, RC und PEIS ermittelt wurden verglichen. Der Fokus der Untersuchungen lag auf der Beeinflussung der Eigenschaften durch Magnesium sowie auf der Suche nach der vorteilhaftesten Substitutionskonzentration. Ebenfalls wurde der Einfluss von Kohlenstoff, welcher zur Leitfähigkeitsverbesserung beigefügt wird, untersucht.

Die Proben konnten mittels Sol-Gel Verfahren in der gewünschten Zusammensetzung synthetisiert werden. Es zeigte sich, dass Magnesium elektrochemisch inaktiv in dem untersuchten Potentialbereich ist und daher als Substitutionselement zulässig ist. Strukturstabilisierung mittels Magnesiums wurde erreicht. Diese zeigte sich in höherer Coulombsche Effizienz, sowie höheren spezifische Kapazitäten im kathodischen Bereich. Weiters wurde herausgefunden, dass der Kohlenstoffgehalt sowie die daraus resultierende Leitfähigkeit eine große Auswirkung auf die elektrochemischen Eigenschaften haben.

Abstract

The energy demand is growing, and the world starts to focus on renewable and sustainable power sources, which strongly depend on nature. As technologies as electricity from water, sun and wind depend on our nature, storage facilities become an important aspect in research. Lithium-ion-batteries (LIB) are among the used materials for electric energy storage and consumer electronics. Improvements of LIB can be made by enhancing the electrode materials' properties such as specific capacity, discharging current and discharge voltage. One material combining high values in those aspects is lithium vanadium phosphate (LVP) which was investigated in this thesis.

However, the downside is, that LVP suffers from rapid capacity decrease while continuous cycling. A promising way to enhance the electrochemical properties is by metal doping. In this thesis Mg^{2+} was used to substitute V^{3+} ions within the phosphate base structure. LVP with a magnesium concentration of 0, 0.016, 0.037 and 0.053 was synthesized successfully. Additionally, in-situ carbon coating with sucrose was done to increase the electronic conductivity.

Experiments with TG-DSC, ICP-OES, Cilas, XRD and BET were conducted to determine the physicochemical properties. The electrochemical properties were investigated by measurements with CV, GC, RC and PEIS.

The results show that magnesium enhances the electrochemical properties such as coulombic efficiency and specific discharge capacity for cathode application. Further the influence of carbon for the electronic conductivity is of great importance.

Table of content

Table of Figures

1 Introduction

Energy demand is growing in an aspect of importance in human evolution. As the energy demand increases, low-emission or sustainable, "green" energy sources become more important. Conventional technologies, i.e. fossil fuels, coal, methane gas or biomass are expected to be replaced by renewable resources such as water, wind, solar and geothermal energy. However, these technologies strongly depend on our nature, thus the demand and supply are fluctuating. This can be minimized by electrical energy storage. Lithium Ion batteries (LIB) are considered to be an effective energy storage. The state-of-the-art technologies rely on lithium-cobalt-oxide which is used as an active material for the positive electrode.

Phosphates based cathode materials are considered as a promising candidate for cathode materials as they combine bigger pathways for Li^+ ions because of the size of the anion and the stability of phosphates. Since 2002 the number of publications on the topic of lithium vanadium phosphate ($Li_3V_2(PO_4)_3$ - LVP) has been growing. Standard LVP suffers from low electronic conductivity (~10^{-8} S/cm) and low cycle stability at higher charge and discharge rates when all three Li^+ ions are extracted. Different approaches have been attempted to improve electronic conductivity and structural and electrochemical stability of LVP such as carbon coating and metal substitution, respectively. In this thesis Mg has been used as substituting material resulting in the formula ($Li_3Mg_xV_{(2-2x)/3}(PO_4)_3$) whereas [0<x<0.5].

In this work several techniques such as x-ray powder diffraction (XRD), thermogravimetrically analysis (TGA), particle size determination (SILAS), scanning electron microscopy (SEM) inductively coupled plasma optical emission spectrometry (ICP-OES), Potentiostatic electrochemical Impedance spectroscopy (PEIS), Cyclic Voltammetry (CV), Galvanostatic Cycling (GC) and electronic conductivity have been used to define the synthesized materials' physicochemical and electrochemical properties.

2 Theoretical background

Rechargeable Lithium Ion Batteries (LIB) are the state-of-the-art components of our portable lifestyle including telecommunication, computing and entertainment. Future LIBs used in hybrid electrical vehicles (HEV), electric vehicles (EV) and stationary energy storage need more advanced electrode materials which have fast charging and discharging capability, high energy density, long shelf-life, high safety issues, easy production and are environmentally friendly. In the past decades, adapting to the increasing need of power and capacity, the chemical energy storage slowly emerged from lead-acid over Ni-Cd and Ni-MeH- batteries to LIB, which are now replacing the Ni-Cd batteries. The big breakthrough might be yet to come. Starting at the beginning there is the need for a definition of the technical concept of "a battery".

2.1.The Lithium-Ion-Battery (LIB)

A battery is an electrochemical cell which converts chemical into electrical energy and vice versa. Two types of batteries exist, those are primary for one-time use and secondary – rechargeable ones. For lithium both types exist and therefore the distinction between Li-battery also referred to as "Li-metal-battery" and Li-ion-battery must be explained. A Li-metal battery is a disposable one-time use battery with an operating voltage from 1.5 to 3.7 V using Li-metal (where the name is derived from) as negative pole which acts as an anode when discharged. On one hand the most common uses of Li-metal batteries are as artificial cardiac pacemakers and automatic external defibrillators where either high energy must be provided in a moment's notice or reliability for many years and small currents are necessary. On the other hand, LIB are electric power sources rechargeable up to many thousand times for portable electronics with a high energy density, less memory effect and low self-discharge. The first to be commercialized LIBs were a system of lithiumcobaltoxide ($LiCoO_2$) and Graphite anode Sony in June 1991[1]. The cell contains a negative electrode (anode), a positive electrode (cathode) and electrolyte. In a pristine cell the Li^+ ions are hosted in the cathode. After that the host shifts from anode to cathode depending on the state of charge. In a charged LIB the anode is the Li^+-ions' host. The cathode is the sink for the Li^+ ions. The electrolyte is the transport medium, providing mobility for the Li^+ ions, connecting and moistening cathode and anode side, which are separated by a membrane. The cell potential (V) and the capacity (A*h/kg=mA*h/g) are directly linked to the chemical structure and materials used in the battery. The amount of stored electrical energy, mostly expressed by weight (W*h/kg), is the key benchmark for batteries and the reason sales of LIBs are striving and they receive much attention in respect of research.

The cell voltage *E* is determined by the difference of the chemical potentials between anode and cathode (the Gibbs Energy of Formation ΔG), represented by the Equation 2.1-I:

Equation 2.1-I Relation between Gibbs Energy of Formation and cell voltage (Nernst potential)

$$\Delta G = -E * F$$

- *ΔG...free reaction enthalpy [kJ/mol]*
- *E...Nernst Potential [V]*
- *F...Faraday constant F=86485.3329 A*s/mol*

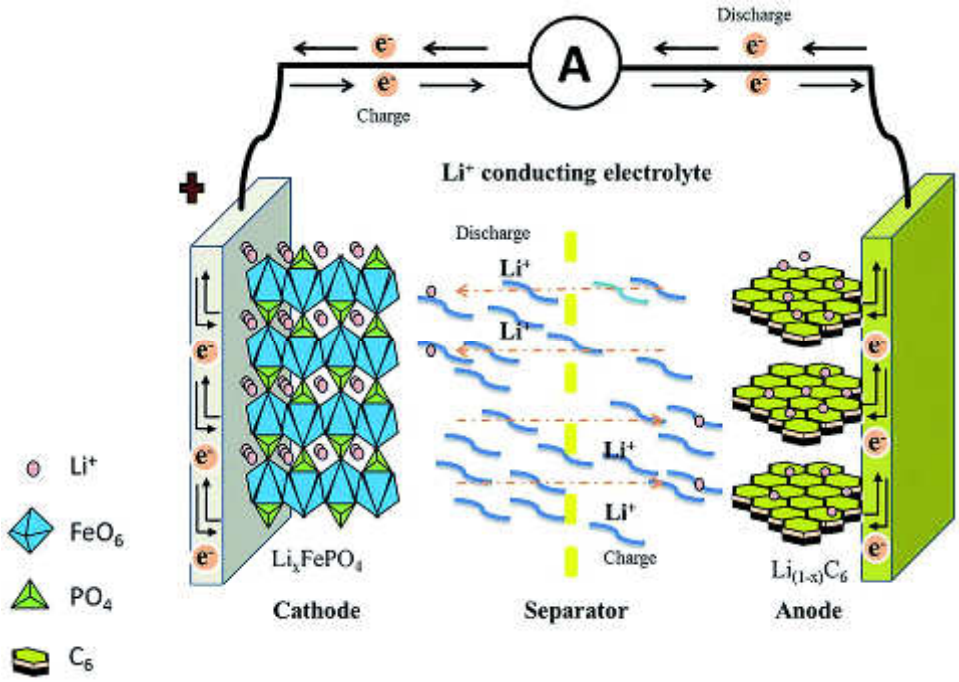

Figure 2.1-I Scheme of a LIB containing lithium ferro phosphate and graphite [2]

Li which is stored in the anode (graphite as pictured) is oxidized to Li^+ while releasing an electron when the battery is discharged.

$$Li \rightleftharpoons Li^+ + e^-$$

The mobile Li^+ ions travel through the electrolyte, a liquid solution of dissociated salts, to the cathode while the electron travels through the external circuit. The oxidation state of the central atom (mostly a transition metal) of the cathode is reduced at the same time, equivalent to the amount of Li oxidized.

Equation 2.1-II Faraday's law

$$n = \left(\frac{I * t}{F * z}\right)$$

- *n...amount of reacted lithium [mol]*
- *I...current [A]*
- *t...reaction time [s]*
- *z...number of transferred electrons [ ]*
- *F...Faraday constant F=86485.3329 A*s/mol*

Those reactions demand good electronic and ionic conductivity for both electrodes. Most commonly used active materials do not fulfill this requirement, which makes it necessary to add electronically conductive materials, such as carbon black, to improve the electronic conductivity. A binder is added to ensure mechanical stability of the whole electrode framework. The reaction takes place within the electrode, where electrolyte, carbon coating and active material meet. For fast reaction rates, resulting in fast charge and discharge the reactions must occur at different

spots at the same time. Therefore, electrodes with porous structures or complex coated networks are favorable due to wider channels, larger active surface resulting in better kinetics. For application and use a suitable sealed casing, such as a coin cell steel package, must be provided.

2.2.LIB benchmarks

Before the materials are described in detail, the parameters they are compared to must be distinguished. Those are:

1. capacity – gravimetric and volumetric
    a. specific capacity
2. open circuit voltage
3. coulombic efficiency

2.2.1. Gravimetric capacity

Gravimetric capacity is the determination of how much electrical energy can be stored in 1 g of active material. The theoretical capacity is calculated shown in Equation 2.2-I.

Equation 2.2-I theoretical gravimetric capacity

$$Q_{g,theo} = \frac{n * F}{\frac{3600\ s}{1\ h} * M}$$

- $Q_{g,theo}$=*theoretical Capacity [Q]=mAh/g*
- *n...number of electrons per formula unit*
- *F...Faraday constant F=86485.3329 A*s/mol*
- *M...molecular weight [M]=g/mol*

2.2.2. Volumetric Capacity

Volumetric capacity is the determination of how much electrical energy can be stored in 1 cm³ of active material. Therefore, $Q_{v,theo}$ can be achieved either by division of $Q_{g,theo}$ by the material's density or as seen in Equation 2.2-II.

Equation 2.2-II theoretical volumetric capacity

$$Q_{v,theo} = \frac{n * F}{\frac{3600\ s}{1\ h} * \frac{M}{\rho}}$$

- $Q_{v,theo}$=*theoretical Capacity [Q]=mAh/cm³*
- *n...number of electrons per formula unit*
- *F...Faraday constant F=86485.3329 A*s/mol*
- *M...molecular weight [M]=g/mol*
- ρ*...material density [g/cm³]*

The specific capacity presents the value of each cell, so it is related to the actual mass of active material used in that certain cell.

2.2.3. Open circuit voltage (OCV)

A pristine cell without attached resistor shows a certain potential before the first charge. This is the open circuit voltage which is measured vs. Li/Li^+ potential which is -3.04 V vs. SHE. For each combination of anode and cathode materials a certain potential can be calculated.

2.2.4. Coulombic Efficiency (CE)

In addition to the mentioned specific capacity the coulombic efficiency is an important factor for the utility of an electrode material as it is directly related to the efficiency of storage, mobility and reversibility of Li^+ intercalation.

Equation 2.2-III Coulombic efficiency

$$CE = \frac{Q_{dch}}{Q_{ch}}$$

- *CE…Coulombic efficiency [%]*
- *Q_{dch}=discharge capacity [mAh/g]*
- *Q_{ch}=charge capacity [mAh/g]*

2.3.Materials

As this work's research has been conducted on cathode materials, this theoretical chapter focuses on the comparison of different cathode materials, no anode materials are mentioned. According to M. Stanley Whittingham the key requirements for cathode materials to be successfully used in LIBs are the following [3]:

1. *The material contains a readily reducible/ oxidizable ion, for example a transition metal.*
2. *The material reacts with lithium in a reversible manner.*

(a) *This dictates an intercalation-type reaction in which the host structure essentially does not change as lithium is added.*

3. *The material reacts with lithium with a high free energy of reaction.*

(a) *High capacity, preferably at least one lithium per transition metal.*
(b) *High voltage, preferably around 4 V (as limited by stability of electrolyte).*
(c) *This leads to a high-energy storage.*

4. *The material reacts with lithium very rapidly both on insertion and removal.*

(a) *This leads to high power density, which is needed to replace the Ni/Cd battery or for batteries that can be recharged using HEV regenerative braking.*

5. *The material has a good electronic conductivity, preferably a metal.*

(a) *This allows for the easy addition or removal of electrons during the electrochemical reaction.*

(b) *This allows for reaction at all contact points between the cathode active material and the electrolyte rather than at ternary contact points between the cathode active material, the electrolyte, and the electronic conductor (such as carbon black).*

(c) *This minimizes the need for inactive conductive diluents, which take away from the overall energy density.*

6. *The material has high chemical stability, i.e. less to no structure change or otherwise degrade, to over discharge and overcharge.*

7. *The material is be low cost.*

8. *The material is environmentally benign.*

The most commonly and commercially used cathode materials are lithium cobalt oxide (LCO), lithium ferro phosphate (LFP) and lithium nickel manganese cobalt oxide (NMC). The comparison of each material will be discussed later. Figure 2.3-I shows a comparison of operating voltages, practical capacity of different electrochemically active materials for electrodes.

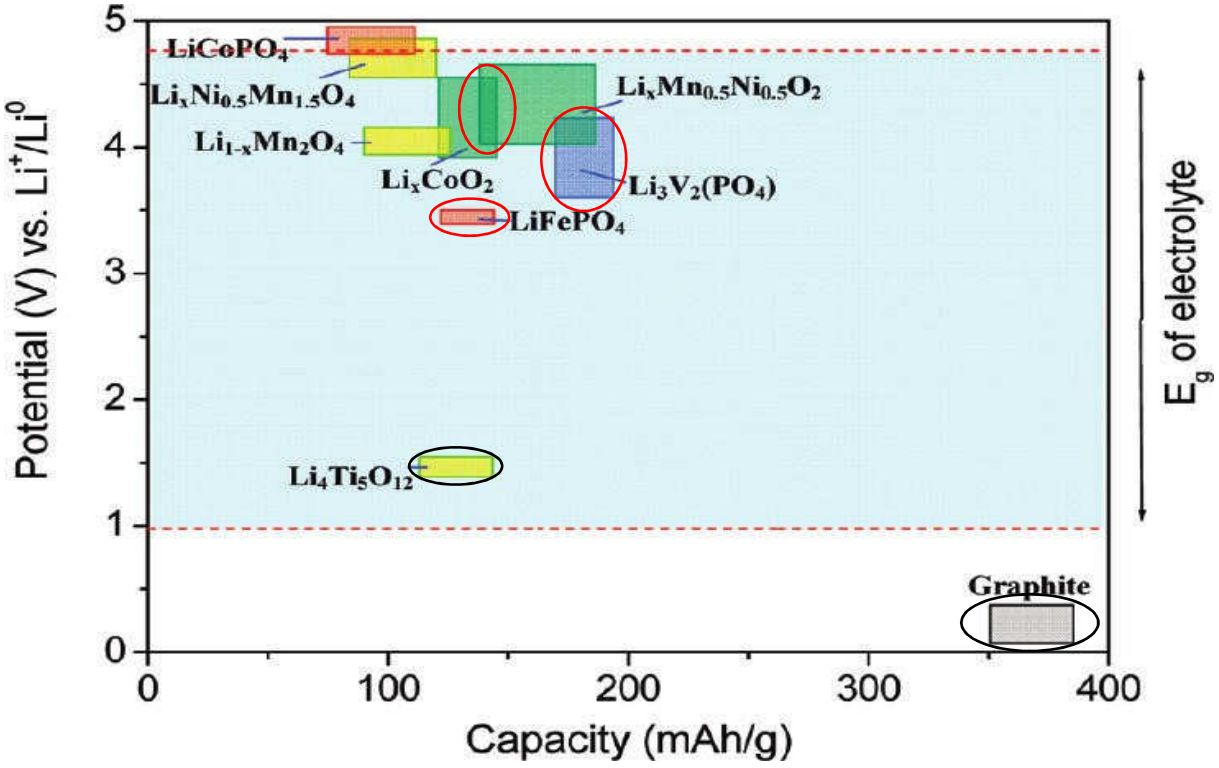

Figure 2.3-I Comparison operating voltages, theoretical capacity of different electrochemically active materials for the later discussed electrode materials in 1 M $LiPF_6$ in EC:DMC 1:1 w/w (taken from Goodenough [4] and edited)

2.3.1. LCO

$Li_{1-x}CoO_2$ (LCO) exists in two different structures: cubic close-packed and hexagonal close-packed. When x=0, oxygen atoms are cubic close-packed arranged while discharging (increasing x) leads to rearrangement towards hexagonal closed-packing of oxygen atoms. Therefore, Li can only be extracted up to x= ~0.5 without change in structure, resulting in lower capacity loss during cycling though lower specific capacity. The low gravimetric energy density is caused by the structure of $Li_{1-x}CoO_2$. The mentioned values are 120-150 W*h/kg at an OCV of 3.6 V [3].

2.3.2. NMC

Layer oxide cathodes such as $LiNiO_2$ (LNO) showed higher specific capacity (275/ 150 mAh/g theoretical/ practical [5]) than LCO (274/ 145 mAh/g theoretical/ practical [6]). However, due to safety reasons such as exothermic oxidation of the organic electrolyte or collapsing of the delithiated structure [7] pure LNO was unfavorable and a mixed oxide structure of $LiNi_{1-x}Co_xO_2$ (LNC) was proposed. Further investigation of possible transition metal oxides showed the advantage of high oxidation states of environmentally friendly, non-toxic and easily available manganese oxide. The spinel $LiMn_2O_4$ (LMO) structure with oxidation states of Mn^{4+}/Mn^{3+} is cheaper than the LCO with only a small deficit in specific capacity. The discharge takes place in a two-step process at 4 V and 3 V regarding to the oxidation stages of manganese of +4 and +3 respectively. Between 1992 and 1999 many variations of $LiCo_xNi_yO_2$, $LiCo_xMn_yO_2$, $LiNi_xMn_yO_2$ whereas x+y=1 have been investigated. The breakthrough came 1999 and 2000, by Liu et.al.[8] and Yoshio et.al. [9] by combining all three transition metals to the now well-known NMC structure $LiNi_{1-x-y}Mn_xCo_yO_2$ [0<x,y<1] with the now used, famous representative NMC333 ($LiNi_{1/3}Mn_{1/3}Co_{1/3}O_2$). This NMC333 or NMC111 exhibits a specific capacity of 150 mAh/g, if cycled between 2.5 and 4.2 V at C/10 [10]. However, NMC has low electronic conductivity (around 6.2-6.8*10^{-5} S/cm) [11] which is a drawback high-rate cathode materials. For NMC 333 initial capacities up to 190mAh/g decreasing to 180 mAh/g at 16th cycle at C/3 in the potential range of 3.0-4.5 V [12]

Influences of the amount of each metal were studied by Ngala et.al. [11], Saadune et.al. [13] and Sun et.al. [14] among others. It is shown that cobalt improves the electronic conductivity while nickel is responsible for structural aspects as layer formation. [13] Increasing cobalt content also leads to higher rate capability [15] because less nickel ions get stuck in the lithium layers. Manganese is crucial for minimizing the costs. The influence can be observed in Figure 2.3-I where the various electrode materials are shown in order of their specific capacity and operating potential. Proposed oxidation states for NMC333 are: Co^{3+}, Ni^{2+}, Mn^{4+} [11].

2.3.3. LFP

Another commercialized safer cathode material is lithium ferro phosphate (LFP) with the molecular structure of $LiFePO_4$.[16] Due to safety issues scientist strived to build safer batteries. One

approach is via polyanionic structures where the metal is octahedrally MO_6 coordinated (where M=Fe, V, Co, Mn, Ni, Ti,...) and polyanions of the structure XO_4^{n-} (where X = P, W, S, Mo,...) [17]–[20], where the anion is tetrahedrally coordinated. In 1997 Padhi et. al. [21] were the first who studied LFP as a substitute for LCO due to the high theoretical capacity of 170 mAh/g, low material costs, natural abundance, environmental friendliness, thermal stability and good cycle stability [22], [23].

2.3.4. LVP

As seen in Figure 2.3-I LVP combines high specific capacity of above 197 mAh/g with a high operating voltage up to 4.6 V [24] thus it is very promising for high voltage LIB. $Li_3V_2(PO_4)_3$ exists in two crystallographic modifications as shown in Figure 2.3-II. The first one (Figure 2.3-II A) is a NASICON (sodium (NA) SuperIonic CONductor) or rhombohedral phase [25] (space group: $R\bar{3}$ a = 8.316(1) Å; c = 22.484(1) Å [26]). The second and thermodynamically more stable structure (Figure 2.3-II B) is monoclinic [27] [28] (space group P21/n; a = 8.605(1) Å; b = 8.591(1) Å; c = 12.038(1) Å) and β = 90.60(1)° [16] in mostly cited non-standard settings). Non-standard means a shortage in b value to nearly 90° connected to a shortage of the c-parameter. The standard setting is $P2_1/c$ with a = 8.605 Å; b = 8.596 Å; c = 14.732 Å) and β = 125.20°[29]

The vanadium sites are not exchangeable having an average V-O bond lengths of 2.003 Å and 2.006 Å [27]. Yin et.al. [27] investigated the three different Li sites via Li-NMR spectroscopy (shown in Figure 2.3-II B). Li(1) is a tetrahedral site whereas Li(2) and Li(3) are pseudo tetrahedral with additional Li-O bond of 2.6 A length.[30]

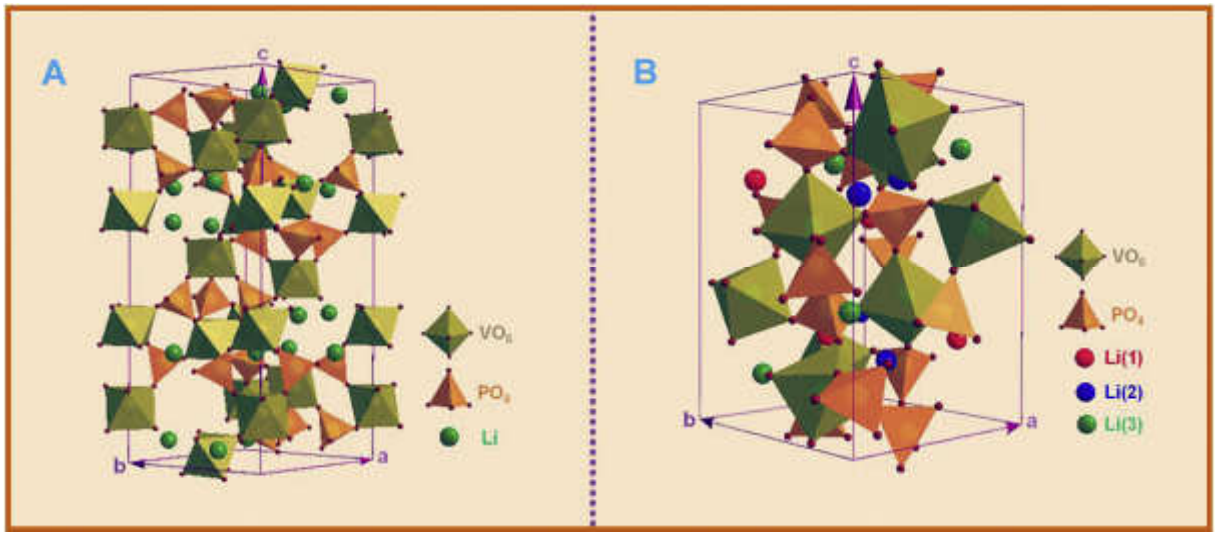

Figure 2.3-II different LVP modifications: A: (left) NASICON; B: (right) monoclinic [31]

The monoclinic LVP has three stable modifications named in order of temperature stability: α-phase (up to 400 K), β-phase (400-460 K) and an orthorhombic γ-phase (460-570 K). The changes between the modifications are fully reversible in an oxygen-free atmosphere, because starting at 800 K in air vanadium is first oxidized from the V(III) state to V(IV) state and later to V(V) state [32].

The main difference in electrochemical behavior between rhombohedral and monoclinic phases is the possibility of Li^+ extraction. In the rhombohedral phase Li^+ extraction functions as a one-step two-ions process. On the other hand, in the monoclinic phase all Li^+-ions are mobile. Figure 2.3-III shows the electrochemical voltage-composition curve for Li^+ extraction in the voltage ranges of (3-4.8 V (A)) which equals the extraction of three Li^+-ions and the voltage ranges of (3-4.3 V (B)) which equals to the extraction of two Li^+-ions. All $Li_xV_2(PO_4)_3$ phases (x = 3, 2.5, 2, 1 or 0) are stable. The extraction of the last lithium ($LiV_2(PO_4)_3$ → $V_2(PO_4)_3$) is found to be the most difficult due to the reduced electronic and ionic conductivity of the emptied $V_2(PO_4)_3$ network [27]. This reaction results in a volume decrease of 7.8 % [27] whereby the monoclinic symmetric does not change. While lithiation the cell parameters are regained and thus prevents the material from fast degradation while cycling. Yin et.al. found out, that both vanadium sites show an alike V-O bond distance and share an average oxidation state of $V^{4.5+}$ [27]. When discharging, this results in disordered lithium insertion which is presented as the s-shaped curve (seen in Figure 2.3-III (A)) pointing out the solid solution behavior. As soon as a composition of $Li_2V_2(PO_4)_3$ is reached, orientation of the phases starts, resulting in a two-phases, two-step insertion of the third Li^+ ion. For the two Li^+ ion process (as seen in Figure 2.3-III (B)) (3-4.4 V) no volume contraction is observed, resulting in order two-phase extraction and insertion while charging and discharging respectively. Thus, a lower but more stable specific capacity is found during repeated cycling (~131 mAh/g) [33], [34].

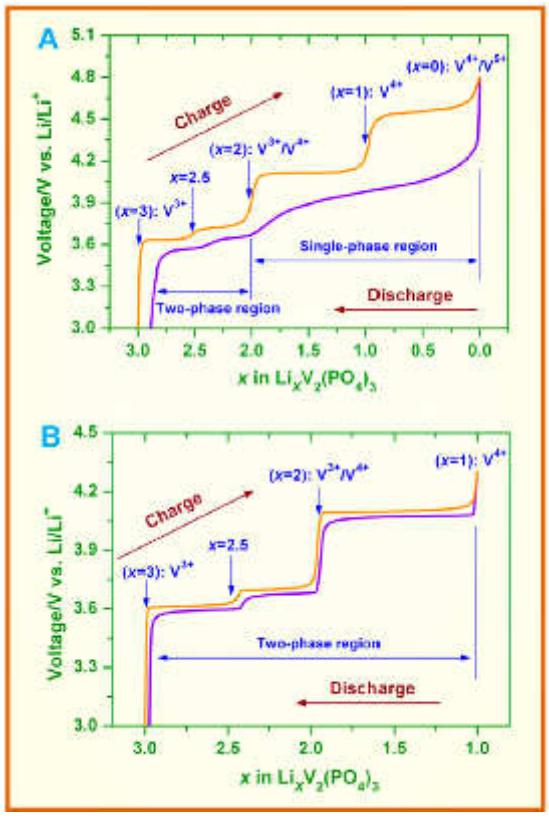

Figure 2.3-III Electrochemical voltage-composition curves of LVP in the voltage ranges of 3-4.8 V (A) and 3-4.3 V (B) [31]

The key factors for great electrochemical performance such as capacity, cycle life and rate capability strongly depend on electronic and ionic conductivity of the electrode materials as well as the Li^+ diffusivity. LVP as a phosphate-based structure has elevated operating potential compared to their oxide counterparts. PO_4^{3-} anions are electronically insulating and isolating the valence electrons of vanadium, leading to low conductivities ($2*10^{-8}$ S/cm[27] and $7.7*10^{-8}$ S/cm[35] – both determined by four-probe conductivity measurements). In relation to previously mentioned LCO ~10^{-3} S/cm[36] or LMO ~10^{-4} S/cm[37] or NMC333 6.2 -6.8*10^{-5} S/cm[11].

2.3.5. Synthesis approaches

A great variety of preparation techniques have been attempted to be effective and expedient to produce LVP for cathode materials for LIB application such as solid-state reaction, sol-gel chemistry, hydrothermal method, spray-pyrolysis, freeze-drying, electrospinning, electrostatic spray deposition and others. Table 2.3-I. shows an overview of used precursors, key issues of the preparation technique, (dis-)advantages and the cited literature. In this thesis, the measured samples were prepared by a sol-gel method combined with auto-combustion. The procedure will be explained in detail in 3.1.

Table 2.3-I Comparison of synthesis approaches for LVP

Preparation technique	precursors	key issues	advantages	disadvantages	reference
Solid-state reaction (SSR)	LiF, Li_2CO_3, CH_3COOLi V_2O_5, NH_4VO_3 $NH_4H_2PO_4$, $(NH_4)_2HPO_4$ acetylene black, glucose	solid precursors are ground / ball-milled heat treated under Ar / slightly reducing atmosphere 1st 300-400°C for gas emission 2nd 600-1000°C	smaller particle size (~300 nm) simple, suitable for mass production	long calcination temperature inhomogeneity, irregular morphology, uncontrollable particle growth, agglomeration,	[38], [39]
Microwave-assisted SSR	as above	electromagnetic radiation leads to heating from the material itself shorter reaction-time	faster, less particle growth cleaner, energy efficient higher reversible capacity,	small scale	[40]
Sol-gel	H_20, polyethyleneglycole, glycole LiF, Li_2CO_3, $Li_xH_yPO_4$ (x+y=3) V_2O_5, NH_4VO_3 chelating agents (citric acid, EDTA + HNO_3, oxalic acid, glycine combustion agents as NH_4NO_3, $(NH_4)_2CO_3$	conversion of a colloidal suspension / solution (*sol*) into an interconnected 3D network with sub micrometer pores (*gel*) temperature treatment @500-900°C for 6-15 h	homogenous mixing at atomic/molecular level, low synthesis temperature (sol-gel), smaller particle size, narrow particle size distribution	two-step process: sintering necessary not suitable for industrial scale susceptible to deviations from process (e.g. evaporation speed)	[41]–[44]

hydrothermal	Polyethyleglycol, H_2O, ascorbic acid, Li_2CO_3, $Li_xH_yPO_4$ (x+y=3) V_2O_5, NH_4VO_3	precursors are dissolved in H_2O and heated in a sealed Teflon lined autoclave	simplicity, homogeneous products, narrow particle-size distribution, morphology control, fast kinetics, short processing time, phase purity, high crystallinity, low cost	Batch process, not easy upscaling	[45]

To improve the low conductivity of LVP, carbon coatings have been using citric acid, glucose, polyvinylidene fluoride and starch as the carbon sources [46]. Rui et.al. research showed that a carbon content of 11,6 w% provides the best electrochemical properties [43], hence Jiang et.al. [47] found 7,7 w% to be the most promising value. In this thesis carbon coated LVP will be further referred to as LVP@C.

Wang et.al. [19] proposed the reason for capacity fading of LVP in the potential range of 3.0-4.8 V, in which the structural change occurs during complete delithiation of LVP. An attempt to control and to minimize the effects of structural change is via doping vanadium positions with transition metals with the same ionic radius as V^{3+} such as Fe^{3+} [48], [49] Co^{2+} [48], [50], Cr^{3+} [51], Mn^{2+} [52], Ni^{2+} [53], Al^{3+} [54], Ce^{3+} [55] and Mg^{2+} or Mg^{2+} and Ti^{4+} co-doping [56]–[58] and many others. The comparison of the electrochemical performance of LVPs with different dopants can be seen in Table 2.3-II. Another approach is the insertion of sodium or calcium into interstitial or Li^{+} positions inducing stabilization through the electrochemically inertness in the desired potential range [53]. Substitution can either stabilize the host structure via elements which are not electrochemically active in the same potential region as LVP, or affect particle size and particle size distribution [57], or conductive and electrochemical properties.

Table 2.3-II Comparison of substitution elements of LVP

dopant	optimized composition (carbon content)	electrochemical performance	references
Fe^{3+}	$Li_3V_{1.98}Fe_{0.02}(PO_4)_3$@C (1 w%)	3.0-4.9 V: 126 mAh/g (80 cycles) at 0.2C	[48]
	$Li_3V_{1.95}Fe_{0.05}(PO_4)_3$@C (11 w%)	3.0-4.8 V: 167 mAh/g (50 cycles) at 0.1C 110 mAh/g (50 cycles) at 10C	[49]
Co^{2+}	$Li_3V_{1.85}Co_{0.15}(PO_4)_3$@C (7.4 w%)	3.0-4.8 V: 119.86 mAh/g (50 cycles) at 0.1C	[50]
Mn^{2+}	$Li_3V_{1.9}Mn_{0.1}(PO_4)_3$@C	3.0-4.8 V: 90 mAh/g (4 cycles) at 0.1C	[52]
Ni^{2+}	$Li_3V_{1.96}Ni_{0.04}(PO_4)_3$@C (4.8 w%)	3.0-4.8 V: 106,7 mAh/g (300 cycles) at 10C	[53]
Al^{3+}	$Li_3V_{1.92}Al_{0.08}(PO_4)_3$@C (4.67 w%)	3.0-4.3 V: 119 mAh/g (200 cycles) at 0.5C 3.0-4.8 V: 145 mAh/g (200 cycles) at 0.5C	[54]

dopant	optimized composition (carbon content)	electrochemical performance	references
Mg^{2+}	$Li_3V_{1.8}Mg_{0.3}(PO_4)_3$@C (4.4 w%)	3.0-4.3 V: 127.4 mAh/g (initial) and 116.1 mAh/g (100 cycles) at 1C	[56]
	$Li_3(V_{0.9}Mg_{0.1})_2(PO_4)_3$@C	3.0-4.3 V: 107 mAh/g (initial) and 104.9 mAh/g (80 cycles) at 20C	[57]
Ti^{4+} & Mg^{2+}	$Li_3V_{1.9}Ti_{0.05}Mg_{0.05}(PO_4)_3$@C	3.0-4.8 V: 147 mAh/g (initial); 121.1 mAh/g (200cycles) at 0.5C	[58]

Magnesium shows properties to be a promising candidate as a stabilizing doping element since Mg^{2+} has an ionic radius of (0.65 Å) which is equal to V^{3+} (0.64 Å) [59]. Also, Mg is not electrochemically active in the working potential of LVP (from 3.0-4.9 V vs. Li/Li^+) [60]. As Mg^{2+} does not take part of the reaction and therefore dos not change its ionic radius, it may stabilize the structure and helps regaining the pristine lattice parameters after complete delithiation. Huang et.al. studied $Li_3V_{(2-2x/3)}Mg_x(PO_4)_3$@C (x=0, 0.15, 0.30, 0.45) substances and found out, that the lowest doping concentration showed the most stable discharge capacities with highest capacity retention, due to the similarity to the undoped material and stabilizing effects of Magnesium [56]. Therefore, the question arose, if substitution levels between x=0 and x=0.05 will show even better results. This led to this thesis' main question: "How does Mg-doping influence stability, particle size, capacity, coulombic efficiency and capacity retention of LVP as an electrode material?"

As Mg is not electrochemically active, thus decreasing the specific capacity of LVP, adjusting its amount is of great importance. In this work $Li_3V_{(2-2x/3)}Mg_x(PO_4)_3$@Cwith x=0; 0.015; 0.035; 0.05 have been synthesized and their morphology, structural and electrochemical properties have been studied. The proposed influence is the mentioned ionic radius. As Mg^{2+} does not take part in the reaction and therefore does not change its ionic radius, it may stabilize the structure and help regaining the pristine lattice parameters after complete delithiation.

3 Experimental

3.1. Synthesis

In this work LVP materials were synthesized by sol-gel and combustion methods. The reaction during the synthesis is based on the following Equation 3.1-I (Mg-doped) and Equation 3.1-II (undoped). The first step was forming the mentioned LVP structure by a sol-gel method. There is a charge balance by vanadium content, because of di-valent Mg-ions replacing three-valent vanadium ions.

Equation 3.1-I reaction mechanism Mg doped LVP

$$7.5C_6H_8O_7 + \left(2 - \frac{2x}{3}\right).NH_4VO_3 + 3LiH_2PO_4 + xMg(NO_3)_2.6H_2O + C_2H_6O_2 + (2-2x).NH_4NO_3 \rightarrow Li_3Mg_xV_{\left(2-\frac{2x}{3}\right)}(PO_4)_3$$

Equation 3.1-II reaction mechanism undoped LVP

$$7.5C_6H_8O_7 + 2.NH_4VO_3 + 3.LiH_2PO_4 + C_2H_6O_2 + 2.NH_4NO_3 \rightarrow Li_3V_2(PO_4)_3$$

Equation 3.1-III carbon coating with sucrose under argon atmosphere at 750°C

$$8.C_{12}H_{22}O_{11} + Li_3Mg_xV_{\left(2-\frac{2x}{3}\right)}(PO_4)_3 \rightarrow Li_3Mg_xV_{\left(2-\frac{2x}{3}\right)}(PO_4)_3@C + CO_2$$

3.1.1. Prepared Samples

Table 3.1-I shows the Mg content desired and as-prepared based on ICP-MS measurement.

Table 3.1-I prepared substitution concentrations (with targeted structural formulas)

Sample	Molecular formula	X= Mg (desired)	X= Mg (achieved)	Color used in graphs
Mg0	$Li_3V_2(PO_4)_3$	0	0	Black ■ □
Mg1	$Li_3Mg_{0.015}V_{1.99}(PO_4)_3$	0.015	0.016	Blue ● ○
Mg3	$Li_3Mg_{0.035}V_{1.977}(PO_4)_3$	0.035	0.037	Red ▲ △
Mg5	$Li_3Mg_{0.05}V_{1.95}(PO_4)_3$	0.05	0.053	Green ▼ ▽

3.1.2. Sol-Gel synthesis of LVP

At first citric acid (CA, $C_6H_8O_7$) is dissolved in approximately 20 mL deionized water at 80°C in a beaker heated by a magnetic heater-stirrer from IKA C-MAG HS7. During constant stirring ammonium meta-vanadate (NH_4VO_3) was added to the solution. A color change is immediately visible which is sign of the reaction. After about 10 min NH_4VO_3 should be completely dissolved resulting in a clear blue solution. Afterwards LiH_2PO_4, $LiCH_2COOH$, $Mg(NO_3)_2$*6 H_2O and ethylene-Glycol ($C_2H_6O_2$) are added in the named order. For complete dissolution the vials were washed with deionized water. The resulting solution was evaporated at 80°C during constant stirring. In a separate beaker NH_4NO_3 was dissolved in 10 mL deionized water. It's worth to mention that the amount of NH_4NO_3 was decreased according to the introduced NO_3 groups with $Mg(NO_3)_2$*6 H_2O (see Equation 3.1-I). After the main solution had decreased to ~30 mL and became sticky, it was poured into a ceramic bowl. Then the ammonium nitrate solution is added. The final solution is evaporated until a gel is formed. The heating must not exceed 110°C, because higher

temperatures lead to self-incineration of NH_4NO_3. Keep attention to a high-volume expansion during this process. Afterwards the gel was put into a preliminary heated furnace (Thermo instruments Heraeus) at 500°C for 20 min. Reasonable precaution is needed as the first expends to 4-6 times of the initial volume and afterwards the gel self-incinerates. After 20 min brown powders can be extracted from the oven.

3.1.3. Carbon coating and heat treatment

For a carbon coating, a solution of acetone (60 mL) and water (10 mL) was prepared, heated to 60°C and then sucrose (approximately 2 g) was added by equivalent of 3:1 by weight of brown powder: sucrose. The solution then was further heated at 60°C and evaporated until 20 mL remained. Meanwhile the obtained precursor in the first step was milled in a ball mill (Fritsch PULVERISETTE 6 in an yttrium stabilized zirconium oxide (YSZ) container with YSZ milling balls (milling balls : precursor weight ratio 8:1). The first step of milling was the mixture of the precursor with the acetone-water-sucrose solution for 30 minutes at 300 rpm. Afterwards the mixture was transferred quantitatively in a beaker with washing. The mixture was then dried and evaporated on a heated magnetic stirrer. After drying for 20 minutes in a preheated furnace at 250°C, the drying process is completed.

Afterwards the milling continues with the same grinding medium precursor ratio for 20 min at 400 rpm and 20 min at 500 rpm.

The milled product was finally heat treated at 750°C for 8 hours in a glass tube furnace, as shown in Figure 2.1-I under high purity (6.0) argon atmosphere.

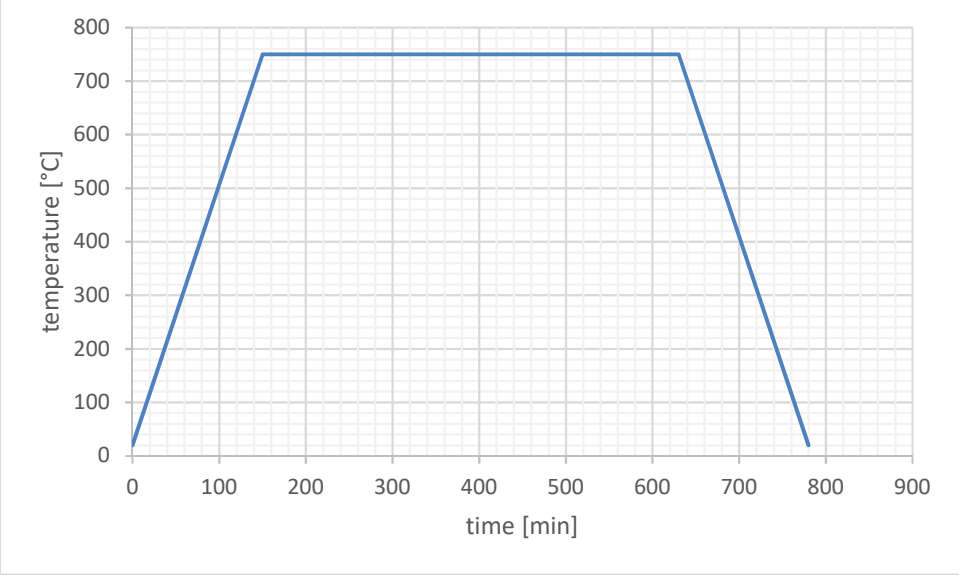

Figure 3.1-I temperature treatment profile T(t)-t, heating/ cooling rate 5°C/s, holding temperature: 750°C, holding time: 460 min

While preparing the carbon coating for the sample Mg5 the sucrose was added directly to the brownish precursor and the diminished acetone-water mixture was poured on top. This led to lower C-content of the sample than the other prepared samples (Mg0, Mg1, Mg3).

3.2. Material characterization

3.2.1. X-Ray Diffraction (XRD)

The crystallinity from the as aforementioned prepared samples was measured with a PANalytical XPert PRO X-Ray Diffractometer. The used radiation was copper-$K_{\alpha 1}$ = 1.5405980 Å at a voltage of 45 kV and a current of 40 mA at a take-off angle of 6.0. The Soller slits were set to 0.04 rad and a fixed incident beam mask of 10 mm. A beta nickel filter with a thickness of 0.02 mm was placed as well. The scan range was set from 3° to 120° (2Θ) with a step size of 0.5°.

3.2.2. Differential Thermal Analysis (DTA)

The differential-thermal-analysis (DTA) is a combination of the two thermal analysis methods (differential scanning calorimetry – DSC and thermogravimetric analysis – TGA). The DTA measurements were conducted with a NETZSCH STA 429 (CD). The used temperature profile is visible in Figure 3.2-I. The experiments were conducted under synthetic air (80 % N_2 : 20 % O_2) heated to 1000°C with a heating rate of 5°C/min and immediately cooled back down to room temperature with a cooling rate of 5°C/min. With the Netzsche program the TG and DTA curves were derivated. Mass loss in the range of 100 - 120°C relates to evaporation of chemically bonded water. From 120 – 200°C some components self-incinerate (as NH_4NO_3 or chlorides) The carbon content was calculated in the temperature range from 280°C - 420°C. At 280°C the decomposition of organic carbon (soil took place and at 420°C the polymers and molecules with higher molecular mass were expected [61].

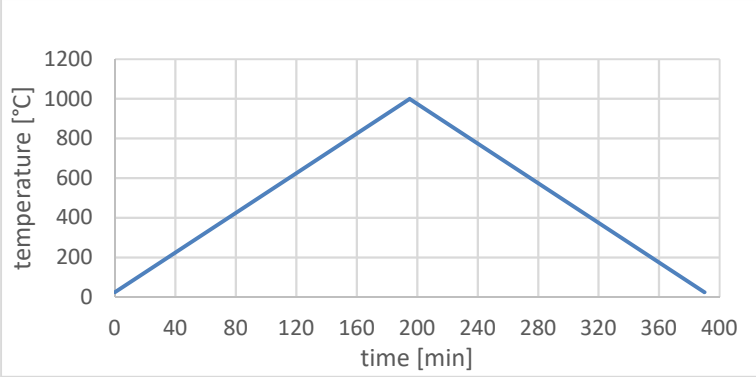

Figure 3.2-I temperature profile (T-t) for DTA measurements

3.2.1. Particle Size (Cilas)

The particle size distributions of the powders were measured based on a light scattering based technique -using Cilas. For sample preparation LVP materials were dispersed in aqueous solutions (since LVP@C is nonreactive with water) using dispersion agent is prepared. Ultrasonic waves were applied to avoid the particle agglomeration. The results were gained comparing scatter

parameters of the monochromatic LASER which revealed the particle size and the particle size distribution therefore gave information of the existence of agglomerates.

3.2.2. Surface and Pore Volume determination by (Brunauer – Emmett – Teller = BET)

The physical functional principal of BET is the adsorption of gas molecules (N_2) on a solid surface below the saturation vapor pressure of the gas. The underlying theory published in 1938 by Stephan Brunauer, Paul Hugh Emmet and Edward Teller, whereas the name derives from.[62] Therefore, the method allows calculation of a mass-related specific surface area. The used procedure followed the DIN-ISO 9277 [63]. The sample was first heated under vacuum to remove water, residues and gas. Afterwards the sample was cooled down to 77 K. The mesoporous surface was measured twice once while adsorption and later desorption between 0.05 and 0.3 bar relative pressure at 8 measuring points.

3.2.3. Scanning Electron Microscopy (SEM)

The morphology of the of the materials was characterized by scanning electron microscopy (SEM) which is a common tool to visualize surfaces and particles smaller than 400 µm. The resolution was limited to approximately 10 nm. The measurements were conducted under high vacuum with a VEGA3 TESCAN in Brno, Czech Republic with the friendly help of the research group of Prof. Maria Sedlarikova. Images of the powdery samples were taken in magnification of 500x, 2000x, 5000x, 10000x, 20000x.

To gain knowledge of the distribution of elements, energy dispersive x-ray spectroscopy (EDX) was done. This method is based on the elimination of core electrons which are then replaced by outer electrons, releasing radiation characteristic for the element.

3.2.4. Inductively Coupled Plasma – Optical Emission Spectroscopy (ICP-OES)

The lithium and magnesium content in the sample were quantitively measured by using an inductively coupled plasma optical emission spectroscopy (ICP-OES). The measurements were conducted with an iCAD 6500 ThermoFischer Scientific. For the sample preparation, 50 mg of the samples were dissolved in concentrated nitric acid (65 w%). Then the solution was inserted in an inductively coupled Ar-plasma (~10000 K) where the elements were excited. The emitted light is characteristic for each element. A CCD detector measured the various wavelengths and intensities simultaneously. Each measurement was repeated twice.

There is a chance that Mg occupying interstitial positions of lithium, however the only way to determine the exact positions would be by performing solid-state nuclear magnetic resonance spectroscopy for Li^+ and comparing bond lengths and strengths to obtain knowledge of the coordination which was not possible within the scope of this thesis.

3.3. Electrochemical Characterization

3.3.1. Electrode preparation

For electrochemical characterization of the materials it was necessary to prepare electrodes from the synthesized materials with high reproducibility. In general, the electrode consists of active materials, conductive additives and binder which are coated on a current collector.

In this thesis, the electrodes were prepared of the following recipe. The mixture consisted of LVP as active material (AM), polyvinylidenflouridine (PVDF) as binder, amorphous carbon black (Super P1042) as conductive additive and N-methyl-2-pyrrolidone (NMP) as a solvent. All components were dried in a BÜCHI B-585 vacuum oven under vacuum at 120°C for the P1042 and 80°C for the PVDF prior to mixing. The active material (AM) was synthesized with in situ carbon coating with sucrose (AMCct), the samples already contained (3) 9.5 - 11 % carbon. To ensure reproducible conditions additionally SuperP (P1042 - an amorphous carbon source) was added to the AMCct to reach a total carbon content of 20 % in the electrodes. These components were mixed together in a ratio of AM:CM:Binder = 7:2:1. The precursors and the ball milling balls with the ration of 1:8 by weight were added in YSZ milling bowl and the mixture was ground at 250 rpm for 30 minutes and 5 minutes break which was repeated five times. Then, the homogeneous powders were poured into a beaker and 1.3 mL (200 w%) of NMP was added. The mixture was stirred for around 24 hours.

The slurry was then casted with an AFA-II-Automatic Thick Film Coater from MTI. For anodes a wet thickness of 120 µm was coated on copper, while for cathodes a wet thickness of 90 µm was coated on aluminum. The electrode sheets were then dried in a vacuum oven at 60°C for 24 hours. The coated foils were then rolled at 120°C with an MTI HR01 to create a homogeneous thickness of approximately 0.4 mm. From the dry, coated sheets electrodes with a diameter of 15 mm were punched out, weighed. Each electrode was numbered to relate to its mass of AM for calculation of specific capacity later.

3.3.2. Coin cell Assembly

The dried electrodes were inserted in the MBRAUN glovebox. The coin cells (type 2032) were assembled as seen in Figure 3.3-I. Type 2032 means a diameter of 20 mm with a height of 3.2 mm overall dimension. The electrode was placed with the metallic side facing downwards in the middle of the cell can and wet with approximately three drops of the electrolyte (trade name: "LP30"). The electrolyte used was 120 µL of 1 M $LiPF_6$ in a solution of ethylcarbonate and dimethylcarbonate (EC/DMC 1:1 by weight). Three layers of Whatmann GF/F separator (18 mm in diameter) were placed on top and moistened with the electrolyte. On top a thin lithium metal plate was placed followed by a spacer of 0.9 mm height and two springs. Finally, the top cap with a sealing ring was placed on top and the arrangement were inserted in the MTI press and sealed with a pressure of 50 bars for 10 seconds. The finished cell was wiped clean and the open circuit

voltage (OCV) was measured. If the OCV of the cell did not reach 3.0 V, it was a sign of a broken electrode, or that the cell was short-circuited during assembly.

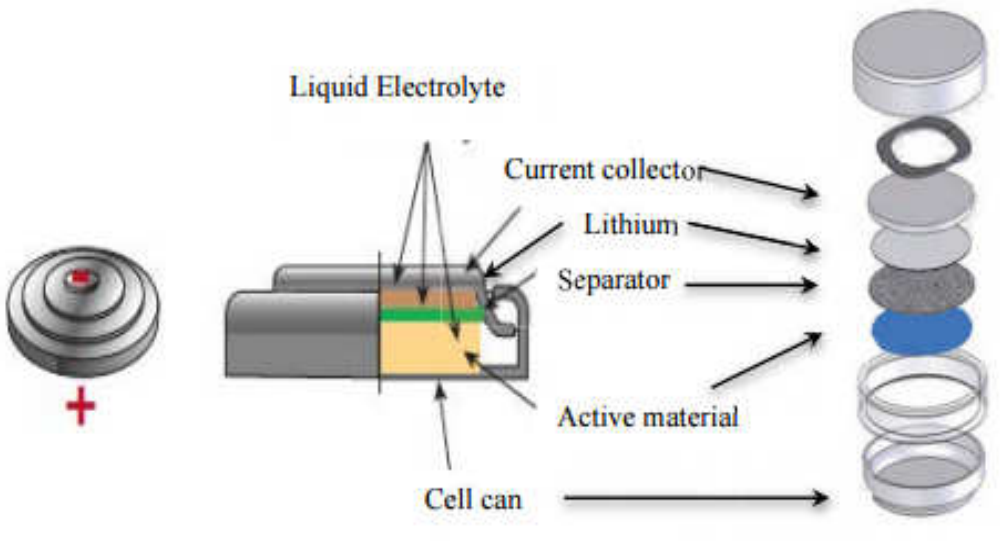

Figure 3.3-I coin cell assembly

3.3.3. Electronic conductivity

The electronic conductivity of the materials was measured by using a four-probe instrument. The setup of the measurements can be seen in Figure 3.3-II and the conductivity was calculated based on Equation 3.3-I. For the measurements round pellets with a diameter of 4 cm were pressed from the synthesized LVP powder with in-situ carbon contains with 4 – 10 tons. After the pressing the pellets were extracted and instantly measured. However, the adhesion of the LVP powder was too low to form stable pellets, thus the length and width of the pellets could not be measured with high certainty resulting in a possibly varying of the electronic conductivity.

The measurement itself was performed within one minute. The pellet was put under the 4 probes and then they were lowered onto the pellet's surface. Then the machine was operated, and the result was written down. Equation 3.1-I was used to calculate with the actual values for the measured parameters (dimensions and voltage) for the calculation of the conductivity.

Equation 3.3-I Conductivity measured by four probes

$$\gamma = \frac{I}{U * h * F\left(h/s\right) * C\left(d/s\right)}$$

- γ...electronic conductivity [
- I...current [A]
- U...Voltage [V]
- h...height of sample [m]
- F...constant dependent on height and distance between electrodes
- C...constant dependent on diameter and distance between electrodes
- d...diameter of the sample [m]
- s...distance between electrodes (10^{-3} m)

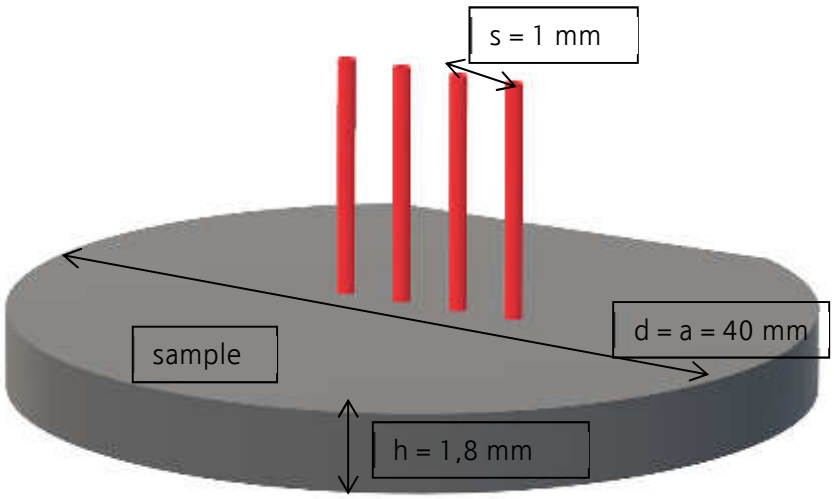

Figure 3.3-II setup of four probe conductivity measurement

3.3.4. Cyclic Voltammetry (CV)

Cyclic voltammetry (CV) is a measurement based on charging and discharging the cell with a constant increase of the potential while measuring the current. The measurements were conducted with a Biologic © VSP potentiostat. To evaluate the data EC-Lab V10.37 © software was used. The conducted measurements were divided into three main groups correlated to a specific set of reactions and therefore a potential range. Those groups (anodic, cathodic, high-voltage) with the correlating peaks can be seen in Figure 3.3-IV. The used slope for all measurements was 0.05 mV/s. An exemplary profile of the potential curve is shown in Figure 3.3-III.

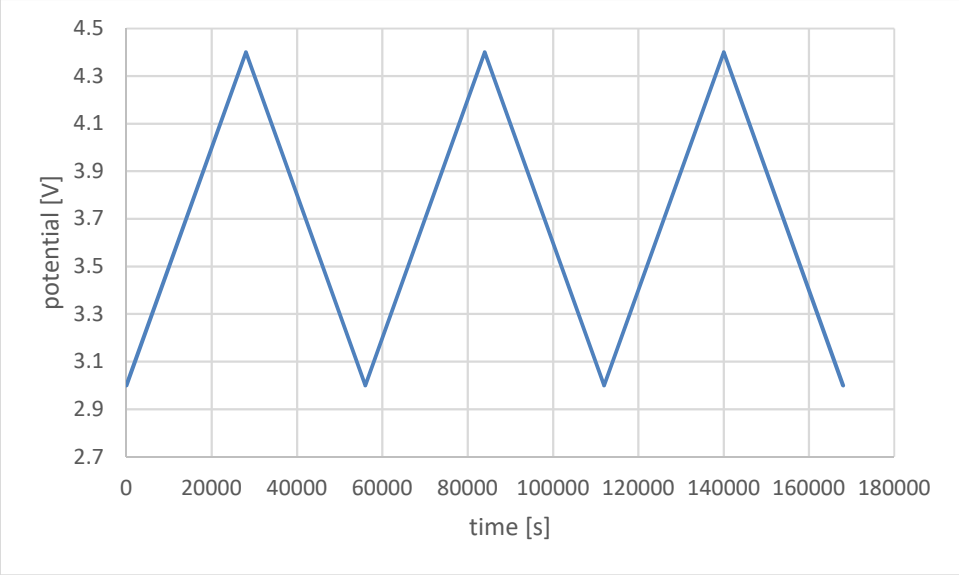

Figure 3.3-III potential profile for CV measurements for the potential range of 3-4.4 V with the scan-rate of 0.05 mV/s

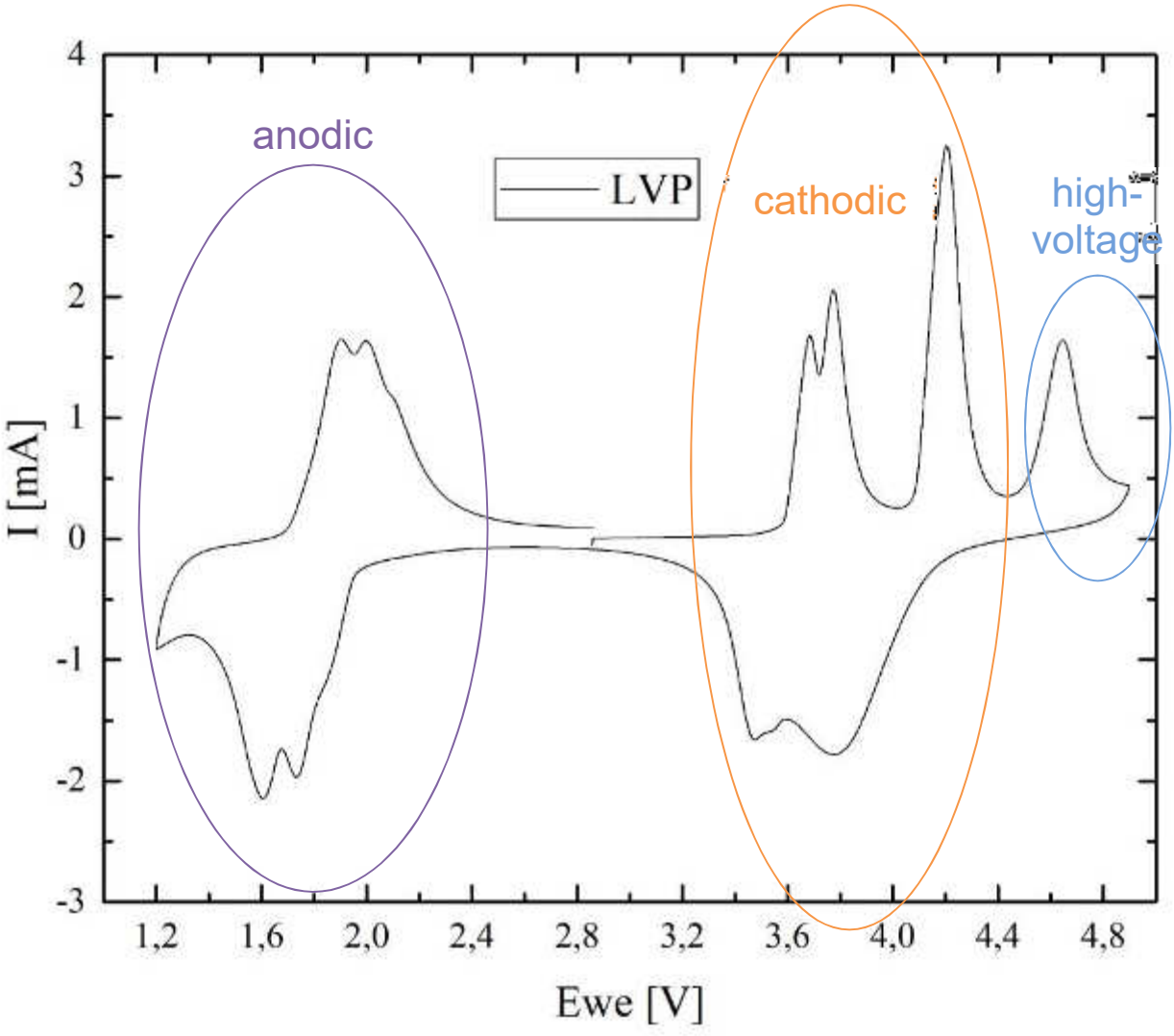

Figure 3.3-IV Cyclic Voltammogram of the LVP in the potential range of 1.2 – 4.9 V vs. Li/Li⁺

Anodic

The samples for anodic operation were investigated in the voltage range from OCV to 1.2 V for charging and a following discharging cycle to 2.4 V vs Li/Li⁺ at a voltage ramp rate of 0.05 mV/s.

cathodic

The electrodes were measured in the cathodic region were charged from OCV to 4.4 V and discharged afterwards to 3 V vs Li/Li⁺ at a voltage ramp rate of 0.05 mV/s.

high-voltage

The high-voltage range covered the charging cycle from OCV to 4.9 V and the following discharging cycle to 3 V vs Li/Li⁺ at a voltage ramp rate of 0.05 mV/s.

3.3.4.1. Linear-sweep voltammetry

A similar technique is LSV. Here the system's potential is altered to a certain potential (either charged or discharged) with a constant ramp rate. This technique was used to reach certain potentials (e.g. 50 % charge of an extraction/insertion peak or to achieve an even potential for all cells.

3.3.5. Potentiostatic Electrochemical Impedance Spectroscopy (PEIS)

The PEIS measurements were conducted with the same Biologic VSP device used for CV measurements, so that the environment did not have to be changed during the experiments.

Electrochemical impedance spectroscopy (EIS) is distinguished into two methods: galvanostatic and potentiostatic mode. In galvanostatic mode the device operates at a constant potential whereas in potentiostatic mode the device operates at a constant current. Usually the received signals are equal but depending on the application one or the other method might be more suitable. E.g. a 10 mV sine wave may lead to an extremely high current (supercapacitors, bigger batteries) or barely no signal (highly resistive coatings or corrosion-resistant materials). The potentiostatic mode is chosen as the conventional approach for smaller batteries. Mostly the measurements are conducted at the open circuit voltage (OCV), which refers the equilibrium state of the newly assembled battery. This state may vary from cell to cell leading to different stages of charge in the beginning. To eliminate these irregularities and standardize the measurement PEIS was measured after reaching determined potentials with LSV. The program used for interpretation, calculation and design of the reference circuit model was ZView©. The used reference circuit model can be seen in Figure 3.3-V. Each electrical element resembles the influence of some reaction. Both Rui et.al. [16] and Shin et.al. [64] used the shown reference circuit model. The values were calculated by adjusting the fit to the measure impedance spectra. The higher the correlation coefficient was, the better the result. The reference circuit model was taken from R1 equals the bulk resistance, whereas CPE2 and R2 equal the double-layer capacity and charge-transfer resistance between electrolyte and Li-metal respectively and CPE3 and R3 are the double-layer capacity and charge-transfer resistance between electrolyte and cathode and CPE1 is equaling Li^+ diffusion.

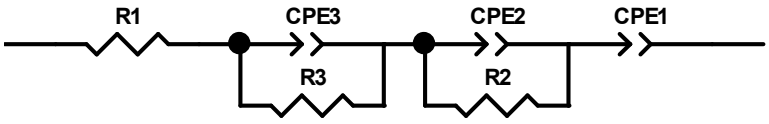

Figure 3.3-V equivalent circuit model

3.3.6. Determination of lithium diffusion coefficient

One important question regarding the influence of magnesium was, if magnesium substitution influences the diffusion coefficients of Li^+-ions and the rate capability. To evaluate this CV was conducted for the first cycle to note each peak and then LSV was conducted for the second cycle. In this second cycle each peak which equals a 50 % charge of this reaction was addressed. At each peak, PEIS measurement was performed to measure the Li^+ diffusivity. Equation 3.3-II used by Ho et.al. [65] was applied. $^{d_E}/_{d_x}$ was calculated from galvanostatic cycling between the 2nd and the 5th cycle via voltage over extracted Li^+-ions.

Equation 3.3-II calculation of Li^+ diffusion coefficient

$$D_{Li^+} = {}^1/_2 * \left[\left(\frac{V_M}{A * F * \sigma_w}\right) * \frac{\partial E}{\partial x}\right]^2$$

- *D_{Li+}...diffusion coefficient of Li^+ ions [cm^2/s]*
- *V_M...molecular volume [cm^3] ($8.9231 * 10^{-22}$) through division of molecular weight and denisty*
- *A...active surface area [cm^2] (1.7671)*
- *F...faraday constant (96486 As)*
- *σ_w...warbourg impedance []*
- *dE/dx...change of current at change of Li^+-ions in grid []*

3.3.7. Galvanostatic Cycling (GC)

Galvanostatic cycling is a method for testing the electrochemical performance of a cell over a long time. The cell was placed in a cell holder and connected to the MACCOR 4000series. In general, those procedures included CCCV charging (constant current until 90 % charge then constant voltage until fully charged) and CC (constant current) discharging with the desired C-rate. Because the dependency of capacity on mass of active material, the weight of the electrodes' active material as well as the equivalent charging current for the desired C-rate was put into the program. The material's theoretical capacity is calculated as shown in Equation 3.3-III. 1 C equals a complete discharge in one hour. The C-rate equals the charging rate. Therefore 1 C means full charge in 1 hour, whereas C/10 equals full charge within 10 hours and 10 C equals full charge within 6 minutes ($1/10^{th}$ of an hour). Obviously, the chemical reactions must take place at an accelerated level to pursue the C-rate. This leads to capacity loss at higher C-rates. Whereas high C-rates are desired because of the required fast charging capability.

Equation 3.3-III C-rate calculation

$$C = Q_{g,theo} * m_{AM}$$

- *C...rate [A]*
- *$Q_{g,theo}$...theoretical, gravimetric capacity [Ah/g]*
- *m_{AM}...mass of active material on the used electrode [g]*

3.3.7.1. Procedures

All procedures start with resting of 6 hours to ensure a chemical equilibrium before the measurement of the cell. Then the first cycle starts with charging (for positive electrodes this means to move towards the higher potential (Li^+ extraction) and negative electrodes towards the lower potential (Li^+ insertion)). Between the two processes, a resting time of 5 minutes was applied.

Cathode 3-4.4 V

Cycling at C/10 between 3.0 - 4.4 V vs. Li/Li^+ for 100 cycles. The first cycle starts with charging the material to 4.4 V which equals to two Li^+ ion exchange process.

Cathode 3-4.8 V

Cycling at C/10 between 3.0 - 4.8 V vs. Li/Li^+ for 100 cycles. The first cycle starts with charging the material to 4.8 V which equals complete delithiation or a three Li^+ ion exchange process.

Anode 1-2.4 V

Cycling at C/10 between 1.0 - 2.4 V vs. Li/Li^+ for 100 cycles. The first cycle starts with charging the material to 1 V which equals a two Li^+ ion exchange process.

3.3.8. Rate Capability test (RC)

Rate Capability tests aim to demonstrate the electrochemical performance and the coulombic efficiency of the material at different C-rates. The tests were performed with the same MACCOR 4000 device. The routine was consecutive CCCV-CC charging/discharging cycles, following the previously mentioned constraints like rest between steps, necessity for active mass per electrode and 6 hours rest in the beginning, with varying C-rates, 10 cycles each. The order was 0.1C, 0.3C, 0.5C, 1C, 2C, 5C, 2C, 1C, 0.5C, 0.3C, 0.1C.

4 Results and Discussion

4.1. Structure analysis (based on XRD)

Figure 4.1-I shows the XRD diffractograms of all samples in comparison to the inorganic crystal structure database (ICSD) file 98-016-1335. The sharp peaks show that the synthesized material is a crystalline and monophasic powder which is easily identified by Highscore Plus© as LVP with a monoclinic $P2_1/c$ symmetry. As seen the peak positions do not vary between samples with or without Mg substitution and the diffraction peak positions match the ICSD standard file, the prepared samples contain no impurities. The lattice parameters were calculated by using Rietveld refinement and the calculated lattice parameters are shown in Table 4.1-I.

Zenyu et.al.[60] observed structural changes (lattice shortage) by substituting $7LiFePO_4$-$Li_3V_2(PO_4)_3$ with magnesium. Therefore, it was interesting whether the same effect could be observed at LVP. Most literature such as Deng et.al.[66], Wang et.al.[19], Kobayashi et.al.[67] and Rui et.al.[31] use the non-standard setting $P2_1/n$ in which β is near 90° and the c-axis is shortened compared to $P2_1/c$. For a direct comparison a transfer is necessary. The obtained lattice parameters ($P2_1/c$) (

Table 4.1-I) match the literature work.

To assess the effect of magnesium substitution on the lattice parameters of LVP, a comparison of each parameter and the Mg content was done, and the correlation was calculated. Lattice b was found to show high a correlation with the magnesium content. The shrinkage the b-axis with increasing magnesium content is due to the ionic radius of two-valent magnesium as well as the shortened Mg-O bond. The shrinkage of b results in the shrinkage of unit cell volume, as well. No correlation was found for the other parameters. A similar effect was observed by Yang et.al.[68] in relation to chromium doping, in which no additional reflexes were found in the XRD diffractogram, indicating that Cr must have entered the LVP structure.

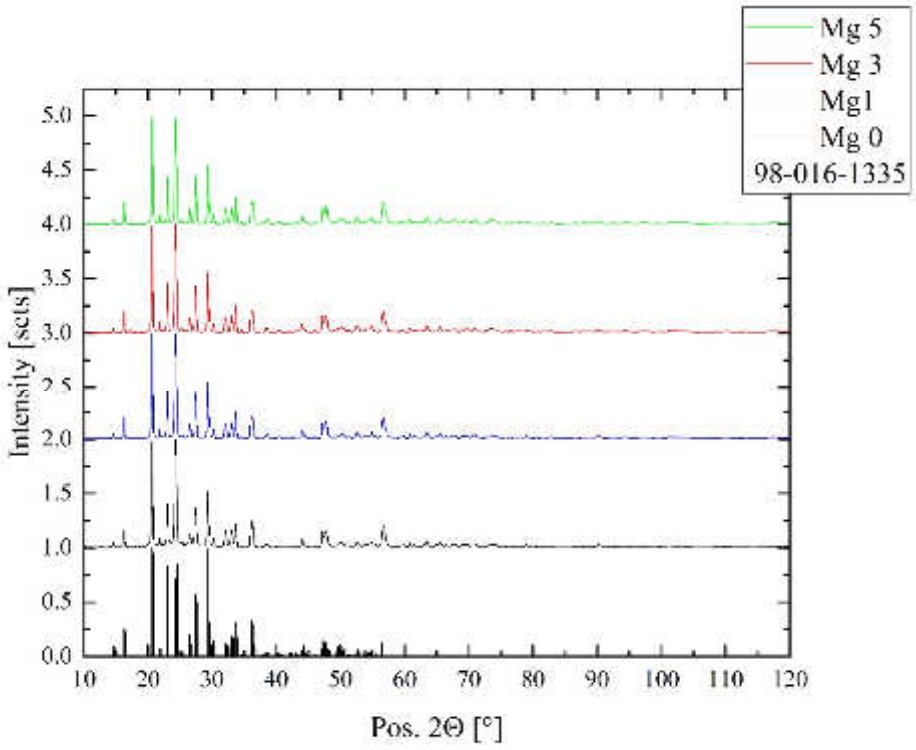

Figure 4.1-I XRD pattern (standardized)

Table 4.1-I Lattice parameters for all samples calculated Rietveld refinement

sample	a [Å]	b [Å]	c [Å]	β [º]	unit cell volume [Å³]	R_{wp}
Mg0	8.60272	8.60229	14.75506	125.2182	892.0569	7.449
Mg1	8.61084	8.59989	14.74395	125.188	892.3089	6.754
Mg3	8.60899	8.59874	14.74301	125.1908	891.9110	6.772
Mg5	8.6066	8.59734	14.74158	125.2074	891.2494	5.407
Correlation	33.3 %	**97.9 %**	84.6 %	24.8 %	**81.6 %**	

4.2. Carbon Content (based on DTA)

TGA was performed to determine the carbon content in the prepared samples. Figure 4.2-I shows the TGA (a) and DTA (b) curves for the prepared samples. At 100-200°C water should evaporate and leftover precursors as NH_4NO_3 self-incinerate. Carbon is oxidized to CO_2 in the temperature range of 300-550°C under synthetic air. Therefore, the measured weight loss corresponds to carbon content. The increase in weight at 600°C and 800°C is related to the oxidation of Vanadium from the 3+ to the 4+ or 5+ form respectively. Table 4.2-I lists the amount of the carbon content for each sample. The sample Mg0.053 shows much less carbon content due to different preparation as previously mentioned.

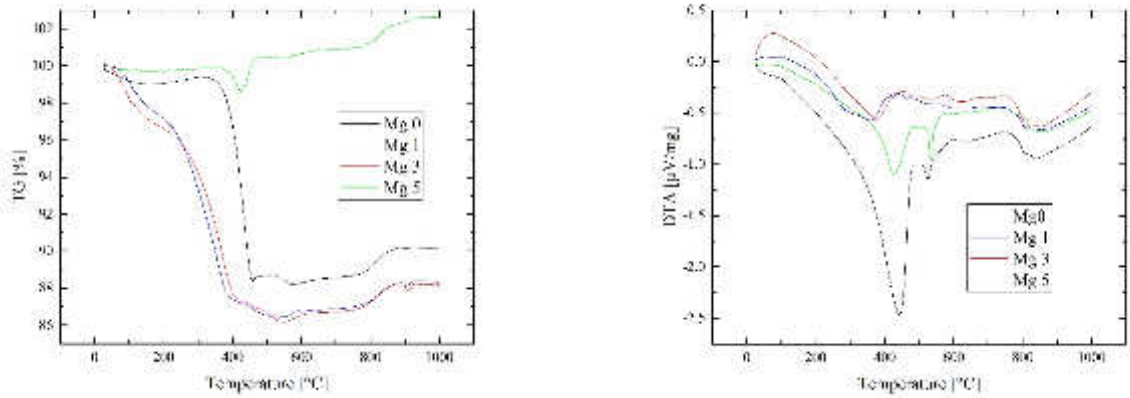

(a) (b)

Figure 4.2-I TG (a) and DTA (b) curves of prepared LVP

Table 4.2-I The amount of carbon content based on TG measurements

Sample	C-content [%]
Mg0	10.97
Mg1	9.91
Mg3	10.32
Mg5	1.93

4.3. The Amount of Mg-substitution and Cations (based on ICP)

To verify the actual composition of the prepared LVP materials, ICP-OES was performed and the results are shown in Table 4.3-I.

To translate the percentages from the raw data (not shown) into an actual composition, determining the norming element to derive the structure from was necessary. This could either be lithium, or phosphate. As phosphate is the structure building component, it seems more adequate as Li^+ ions can take interstitial positions. Therefore, only norming on phosphate is shown in Table 4.3-I. Checking Table 4.3-I shows that vanadium and magnesium together exceed the proposed sum of 2 ions (under the premise that they occupy the same position as required for substitution). The raw data shows an accuracy (relative standard deviation) of around 5 %. This means no actual composition data can be acquired for the LVP structure. Due to the variation of 5 % for vanadium (value is around 2) in the composition, the error is bigger than the total magnesium content. Therefore, the relatively big error span hinders a correct calculation of the composition and enables only the conclusion, that the desired magnesium substitution composition was acquired by synthesis. Further structure related deductions are not equivocally secure.

Furthermore, the given oxidation numbers are theoretical, as ICP-OES is not able to determine the existing oxidation state of the tested ions and elements.

Table 4.3-I ICP-OES measurements of Li, Mg, V and (PO_4^{3-}) – content determination based on ICP-OES

sample	Li^+	Mg^{2+}	V^{3+}	$(PO_4)^{3-}$	M [g/mol]
Mg0	3.037 +/-0.154	0.000 +/-0.000	2.006 +/-0.108	**3.000**	408.16
Mg1	3.056 +/-0.096	0.016 +/-0.001	2.005 +/-0.084	**3.000**	408.66
Mg3	3.054 +/-0.137	0.037 +/-0.002	1.991 +/-0.100	**3.000**	408.41
Mg5	2.996 +/-0.146	0.053 +/-0.002	1.960 +/-0.085	**3.000**	406.84

4.4. Particle Size (Cilas)

As the particle size distribution of the materials has an effect on their electrochemical properties, it is necessary to measure the prepared materials. The particle size measurement shows bimodular distribution for the unsubstituted and substituted samples (shown in Figure 4.4-I (a) and (b)). Bimodular in terms of distribution means two maxima with quite the same height. The particle distribution of all the samples in more detail are shown in Table 4.4-I. It can be seen that 50 % of the particles are smaller than 0.8 µm for the substituted and smaller than 4.135 µm for the unsubstituted, which is a sign of higher tendency of the unsubstituted particles to agglomerate. Combined with the in mentioned results it is clear to say, that the unsubstituted sample has a larger active surface area and bigger particles. As mentioned in Yang et.al.[68] for chromium substitution and various others, the substitution metals positively affect the particle size and agglomeration tendencies, as seen in Figure 4.4-I (b).

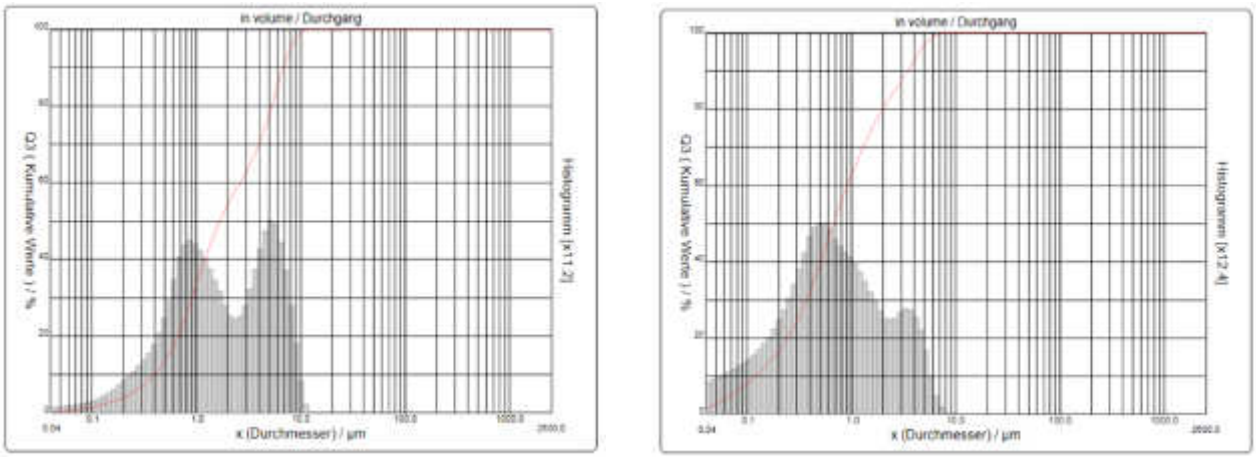

(a) (b)

Figure 4.4-I particle size distribution for unsubstituted LVP (a) and substituted LVP (b)

Table 4.4-I particle size distribution for all samples

sample	Range [µm]		particle size of percentage [µm]		
	from	to	10 %	50 %	90 %
Mg0	0.04	11	0.310	4.135	6.735
Mg1	0.04	8	0.125	0.685	3.450
Mg3	0.04	10	0.195	0.850	3.760
Mg5	0.04	11	0.130	0.625	4.675

4.5. Pore Size, Pore Volume, Specific Surface Area (based on BET)

Besides the particle size, the physicochemical properties such as pore size and the pore volume affect the electrolyte transport and the Li^+ ion diffusion pathway. In this regard, mesoporous materials are defined as materials with the size diameter, which lies between 2 to 50 nm are promising electrochemical materials regarding conductivity and diffusion pathways, which were studied by Eftekhari et.al. [69].

The measured specific surface areas for all samples lie within 23-85 m^2/g. The wide span differs in two regions: 23-32 m^2/g for substituted and 85 m^2/g for unsubstituted samples. For Mg0 a by far higher surface area can be observed due to space within and between the previously mentioned and formed agglomerates. The finer particles of the substituted samples show lower specific surface area and in relation thereto bigger average pore size. Mesoporous materials are defined via pore size diameter, which lies between 2 to 50 nm.

Table 4.5-I specific surface area and pore size diameter

sample	BET [m^2/g]	average pore size diameter [nm]
Mg0	85.29	9.248
Mg1	23.98	18.18
Mg3	23.92	18.62
Mg5	32.28	14.45

4.6. Morphology (based on SEM)

Figure 4.6-I shows SEM images of all prepared samples with different magnifications. The red line in the pictures in the first row show the scale for the respective column. All samples are shown in three magnifications (500 times, 10.000 times, 20.000 times). All samples show homogeneous particles. In the smallest augmentation (500 times), we can see that there are bigger particles with enlarged surface.

The seemingly rough structure grows finer with increasing magnification. Even at 20k magnification no individual particles are visible. For Mg1 and Mg3 (10k) some particles with a diameter of above a diameter of 20 µm are visible. Those flakes are rare.

4.6.1. Elemental Mapping with EDX

From SEM could be taken, that there should be no unwanted elements or impurities as there are neither brighter nor darker spots on the taken images. Those would refer to heavier or lighter elements than the average. Element mapping was conducted by using EDX for C, O, V, P, at the magnification of 500x, a higher magnification was not possible due to resolution issues. The Mg signal was too weak to be measured. Due to the low resolution it could not be determined whether the small particles on the surface are surface-enlarging carbon particles or LVP crystallites.

The elemental mapping (shown in shown in Figure 4.6-II) demonstrates that O, P and V are homogeneously distributed. However, due to low atomic and weight composition of O and C in the samples, the expected errors are high.

Carbon which is shown as a bright red spot was not well distributed in the sample Mg0. Where it looks homogeneous in the Mg1 and Mg3 samples.

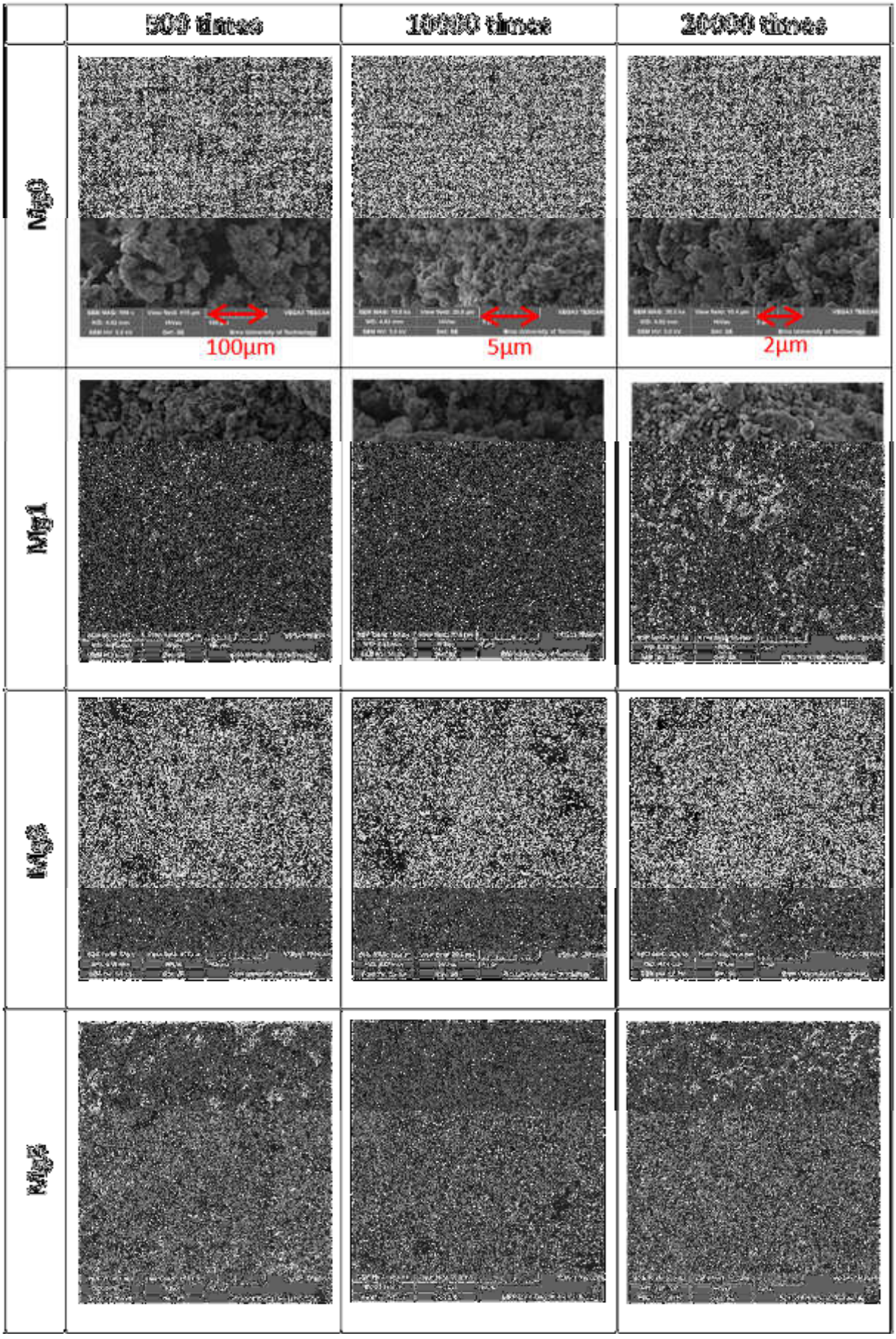

Figure 4.6-I SEM-images of all samples for 500x, 10000x and 20000x magnifications

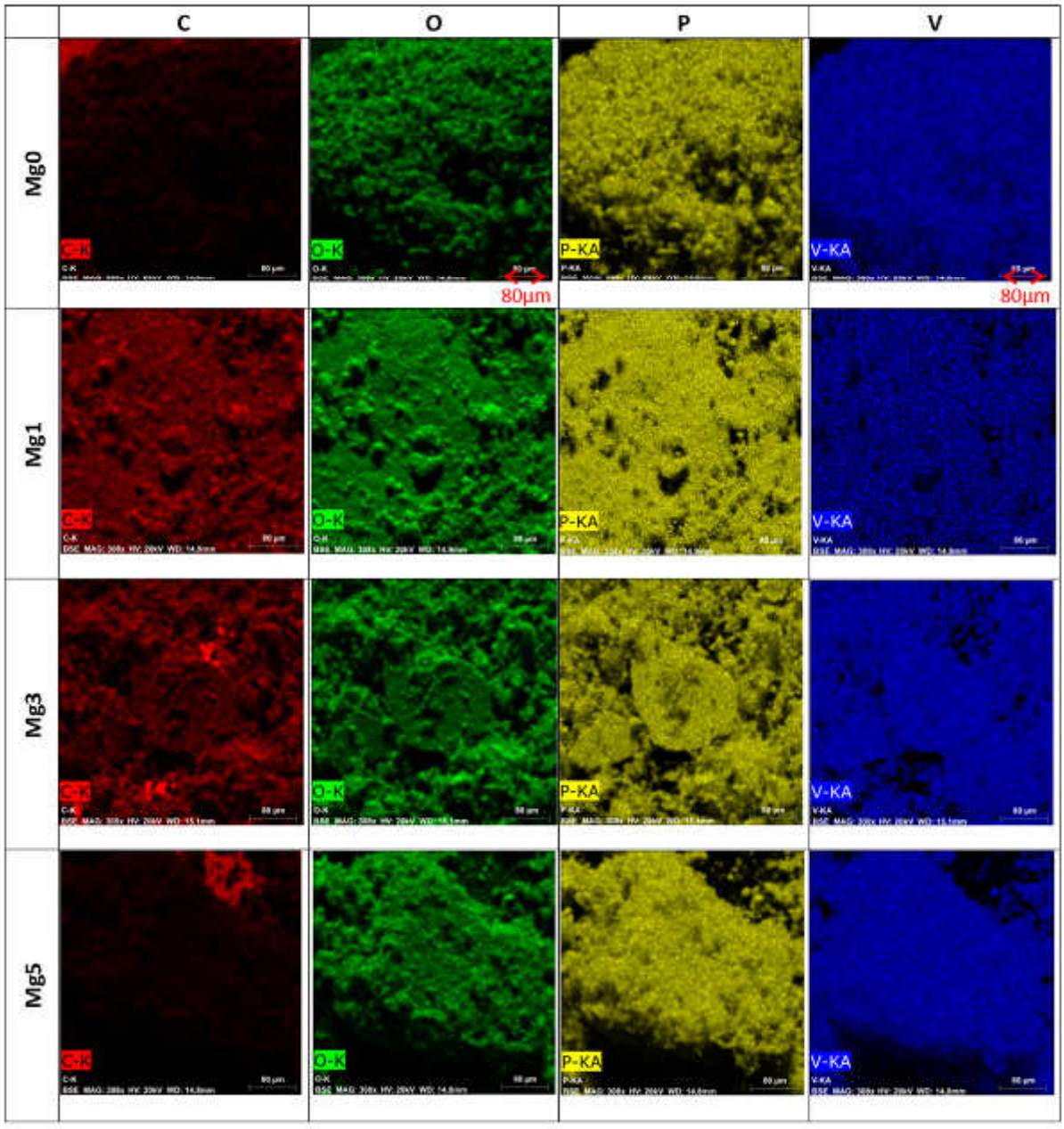

Figure 4.6-II Elemental mapping with BSE and SE for different Mg substitutions at 500x magnification

4.7. Electronic Conductivity

Table 4.7-I lists the electronic conductivity for the synthesized LVP material with different substitution concentration. LVP is known to have a low electronic conductivity ($2*10^{-8}$ S/cm [70]). An increase of the electronic conductivity in the power of 10^6 due to Carbon seems realistic. Some examples for the electronic conductivity for other materials are silver ($6{,}3*10^7$ S/cm), amorphous carbon ($2*10^3$ S/cm), magnesium ($2.3*10^5$ S/cm) or silicon ($1{,}56*10^{-3}$ S/cm) [all [71]] as conductors or semi-conductor respectively. The samples show increasing electronic conductivity by increasing Mg content. A possible explanation for the lower conductivity of the unsubstituted sample, Mg0, is inhomogeneous carbon coating which is shown from EDX mapping in Figure 4.6-II. Unfortunately, the carbon content of Mg5 is only 2 w% due to the before mentioned synthesis error. Therefore, this is by far the lowest carbon coating concentration of all samples. Logically, it resulted in lower conductivity.

Table 4.7-I electronic conductivity of all synthesized materials

sample	I [A]	U [V]	I/U [A/V]	F(s) [ ]	C(d/s) [ ]	h [mm]	**γ [S/cm]**
Mg0	0.001	0.0403	0.0248	1.3863	4.4516	1.8	**0.002**
Mg1	0.01	0.0181	0.5531	1.3863	4.4516	1.8	**0.050**
Mg3	0.01	0.0116	0.8591	1.3863	4.4516	1.8	**0.077**
Mg5	0.0001	0.0625	0.0016	1.3863	4.4516	1.8	**0.0001**

5 Electrochemical material properties

5.1. Electrochemical Results for two Li^+-ion Transfer Cathode Material (3 – 4.4 V vs. Li/Li^+)

5.1.1. Cyclic Voltammetry for LVP materials with different Mg-substitution Concentrations

Cyclic Voltammograms of LVP materials during the first cycle with the scan rate of 0.05 mV/s with the potential range of 3.0 – 4.4 V vs. Li/Li^+ can be seen in Figure 5.1-I. The potentials for interaction of Li+ correlate to the in literature mentioned (shown in Figure 5.1-IV) e.g. Zhu et.al.[42], [66]. For the extraction the given potentials of 3.61 V, 3.70 V and 4.11 V correlate to the measured ones, even though the used scan-rate of 0.02 mV/s was lower. No additional peaks on the substituted LVP materials were observed which indicates that magnesium is not electrochemically active in the tested potential range. Thus, capacity is solely from lithium insertion / extraction processes. Obviously, the peak position varies from one material to another. To verify that if the variation is due to the Mg substitution or the cell preparation, CVs of several electrodes with the same substitution are compared in Figure 5.1-II. We can see that the peak positions vary from one electrode to another which confirms that the preparation of the cells is the reason for the differences.

In Figure 5.1-III the material variation for 5 cycles can be observed moving in the arrow-marked direction. An additional peak at 3.48 V vs. Li/Li^+ can be observed. This peak has occurred several

times at all different substitution concentrations and is not reproducible as it vanishes at repeatedly cycling a cell and did not appear at all investigated cells. One explanation could be that a lithium ion was first inserted to a semi-stable position within the network and later moved to the original position, resulting in capacity and energy loss. The additionally observed insertion peak at 3.48 V, shown as a broad shoulder, was observed and published by Zhu et.al. [42] as well. Despite the in [42] used lower C-rate the scan resolution is smaller, especially for the insertion peaks.

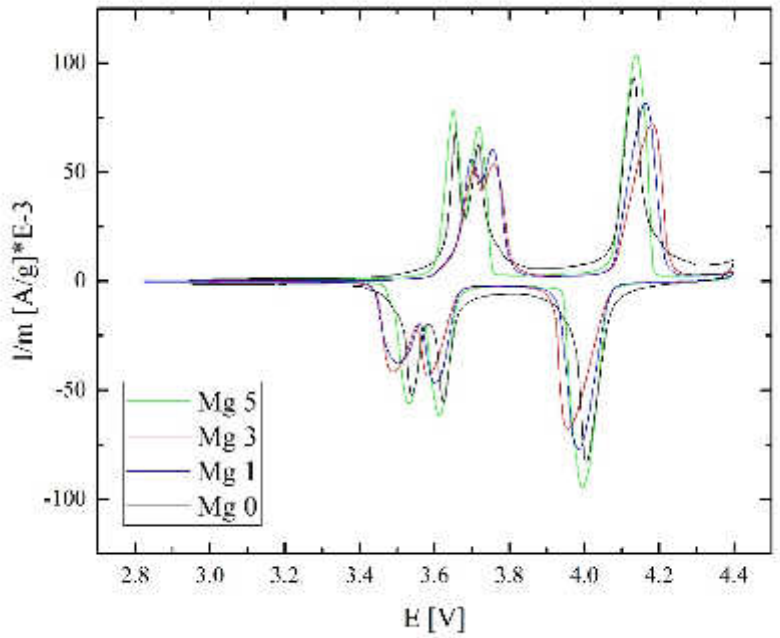

Figure 5.1-I Cyclic Voltammograms of LVP materials during the first cycle with the scan rate of 0.05 mV/s with the potential range of 3-4.4 V vs. Li/Li$^+$

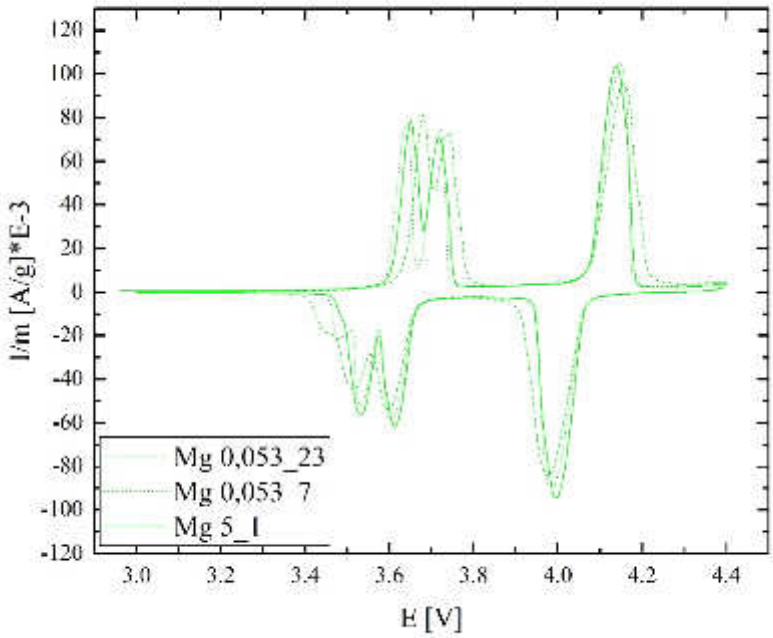

Figure 5.1-II different Mg5 samples scan rate of 0.05 mV/s with the potential range of 3-4.4 V vs. Li/Li^+

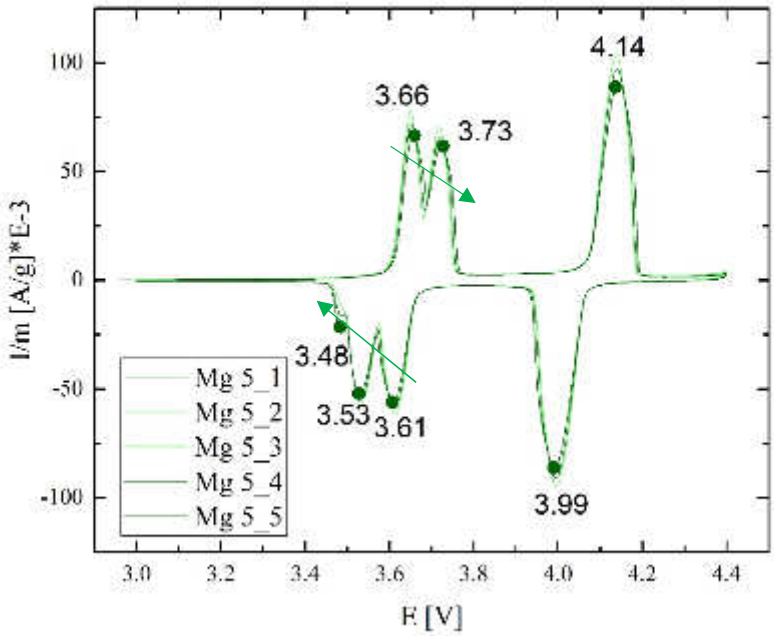

Figure 5.1-III CV for Mg5 for 5 cycles scan rate of 0.05 mV/s with the potential range of 3-4.4 V vs. Li/Li^+

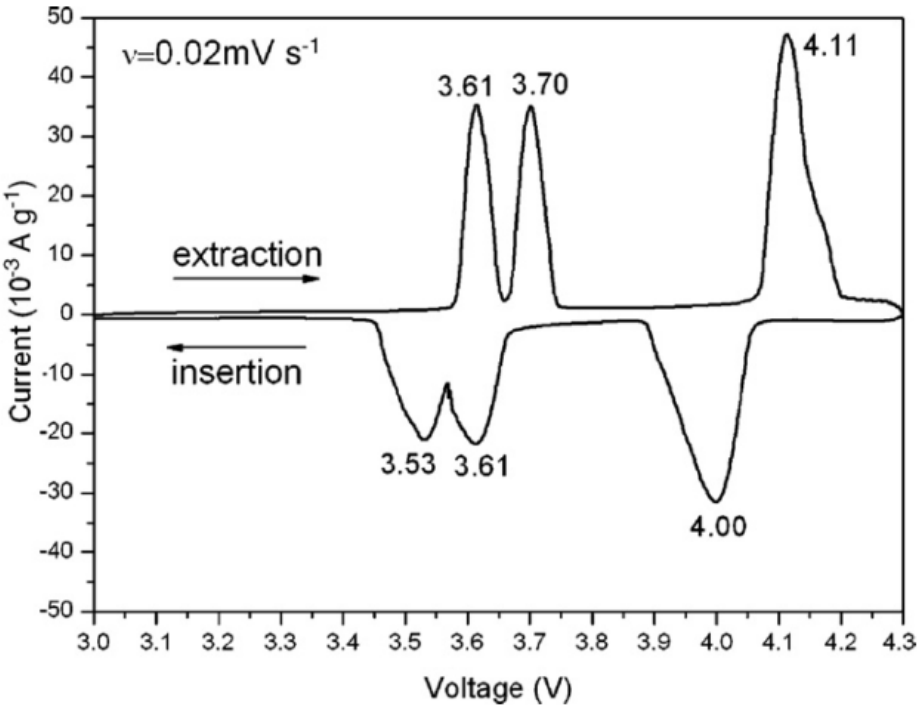

Figure 5.1-IV Cyclic Voltammogram of LVP in with the scan rate of 0.02 mV/s in the potential range of 3-4.3 V vs. Li/Li⁺ reported by Zhu et.al.[42]

5.1.2. Galvanostatic cycling at C/10

Figure 5.1-III shows that magnesium is not electroactive in the examined region. Therefore, the amount of magnesium decreases the maximum available capacity because of its substitution character. Further increasing the Mg content would lead to lower theoretical and practical capacities.

Figure 5.1-V (a) and (b) show data consisting mean values formed out of at least two samples with a deviation from each other below 5 %. The unsubstituted sample (Mg0) exhibits a very poor electrochemical performance throughout 100 cycles. The Mg substituted samples show an improved specific capacity. The specific discharge capacity of all samples for different cycles and the average capacity retention can be seen in Table 5.1-I. The initial discharge capacities of Mg0, Mg1, Mg3 and Mg5 are 124, 122, 118, 124 mAh/g respectively. Above 90 % of the theoretical value were reached in the first cycle. We remind readers that the theoretical capacity of LVP based on two lithium extraction / insertion processes in the potential range of 3 – 4.4 V vs. Li/Li⁺ is around 131 mAh/g [33], [34]. Upon cycling the discharge capacities of all samples decrease constantly. The unsubstituted material shows the highest decrease over the first 10 cycles, nearly 5 % compared to the initial cycle, while the substituted materials' capacity fading is around 1 %. Here Mg3 demonstrates the lowest loss of only 0.7 %. The average capacity retention (10th to 100th cycle) is the best for material Mg1 with 98.2 %. The unsubstituted material shows high fluctuation after 80 cycles resulting the discharge capacity above 87.8 % of the theoretical value

for 100 cycles. These fluctuations were shown in another 10 unsubstituted samples, which can be due to the Li trapping after 70 cycles before sudden release.

The steady and high capacity provided by the substituted samples – mostly Mg1 - demonstrate that the electrochemical performance benefits from substitution with magnesium. The capacity retention from the 10th to the 100th cycle of 98.2 % as seen in Table 5.1-I clarifies that Mg1 shows the best properties.

Table 5.1-I Specific discharge capacitites for 3-4.4 V

Electrode name	discharge capacity at 1st cycle [mAh/g]	Charge capacity at 1st cycle [mAh/g]	discharge capacity at 10th cycle [mAh/g]	discharge capacity at 50th cycle [mAh/g]	discharge capacity at 100th cycle [mAh/g]	capacity retention between 10th and 100th cycle [%]
Mg0	124.21	145.77	119.81	116.41	116.76	97.5
Mg1	122.63	131.39	121.19	119.60	118.98	98.2
Mg3	118.51	126.77	117.68	116.13	115.07	97.8
Mg5	123.52	139.61	121.89	119.77	118.15	96.9

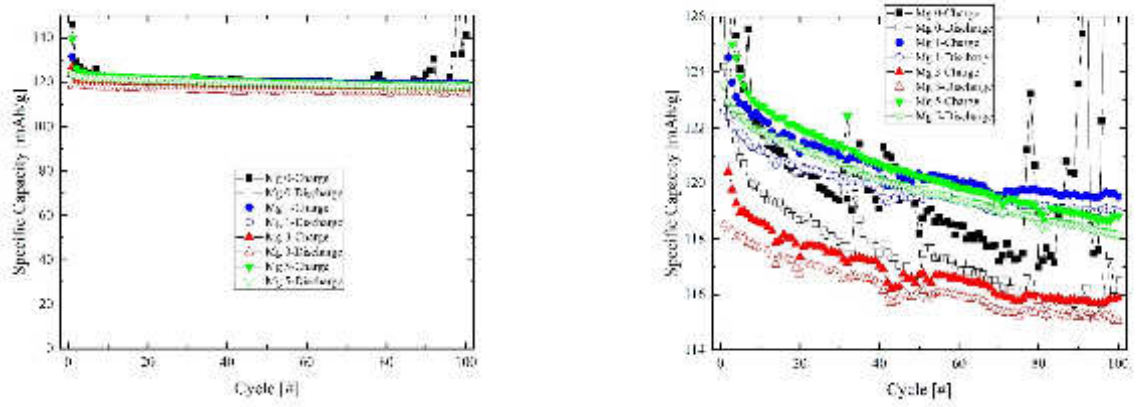

(a) (b)

Figure 5.1-V Specific capacity vs. cycle number for all substitution concentrations in the potential range of 3 - 4.4 V bs. Li/Li$^+$ (a); zoomed at 114-126 mAh/g (b)

5.1.3. Coulombic Efficiency (CE)

Figure 5.1-VI shows the CE vs cycles profiles of the LVP samples with different substitution concentrations. It is clearly seen that the CEs of the substituted samples are higher than those of the unsubstituted. From Figure 5.1-VI (b) it is shown that after 5 cycles, a CE higher than 99 % is reached whereas Mg0 never reaches 99 %. After around 50 cycles CEs above 99.5 % are achieved. CE higher than 100 % can be explained by delayed extraction of the stored Li$^+$, as discussed before. This effect mostly occurs directly after a decline. It can also be seen, that an increase of the magnesium content means an increase of the coulombic efficiency.

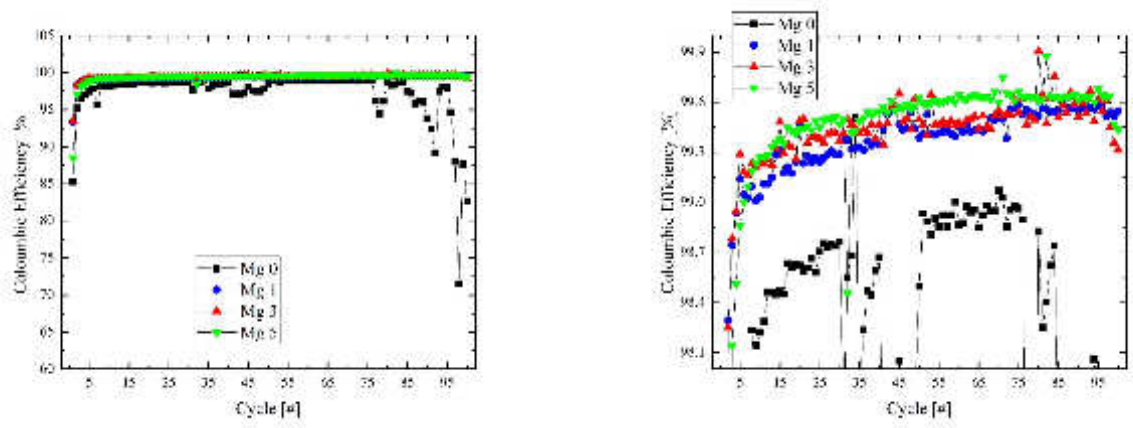

(a) (b)

Figure 5.1-VI Coulombic efficiency vs. cycle number for LVP materials with different concentrations of magnesium in the potential range of 3 – 4.4 V vs. Li/Li⁺ (a); zoomed 98.0 – 99.9 % (b)

5.1.4. Rate capability

Figure 5.1-VII (a) shows the rate capability measurements of all samples in the potential range of 3 – 4.4 V vs. Li/Li⁺ with the C-rate of 0.1, 0.3, 0.5, 1, 2 and 5 C. Even for low C-rates, i.e. 0.1 C and 0.3 C, all materials show differences in respect of specific capacity. With increasing C-rate, the electrochemical performance of the materials diverges, revealing Mg3 as the most promising with the discharge capacity of around 90 mAh/g at 5C, higher than those of Mg1 with 40 mAh/g at 5C. For increasing C-rates for Mg0 the coulombic efficiency decreases, and the discharge capacity nearly completely fades. Mg5 has a complete capacity drop to 0 mAh/g at 5C, but fully recovers with decreasing current and nearly reaches the previously measured capacity. This drop at high C-rates can be explained by reconciling the mistake during preparation, leading to a too low in-situ carbon coating content of ~2 %. At higher C-rates, the low electrical conductivity leads to a large voltage drop which triggers the termination conditions too early. At around 110 cycles the, in GC observed, instability occurs leading to higher charging capacities. This instability might be an effect of cycling at lower C-rate, because neither of the cycled samples showed the symptoms at higher C-rates. The reason might be the termination condition, thus leading to accumulation of lithium.

Coulombic efficiency profiles can be seen in Figure 5.1-VII (b). The substituted materials demonstrate far-higher CEs than the one without substitution However, after 100 cycles the unsubstituted inexplicably exhibits the highest values for coulombic efficiency. It can be assumed that inequalities between charging and discharging (see the low coulombic efficiency for Mg0 in Figure 5.1-VII (b)) at higher C-rates further influences the coulombic efficiency due to stored Li⁺. Further it can be assumed that the effects of Mg-substitution in LVP has higher effects on the higher C-rates rather than on the low C-rates, as observed in studies by Chen et.al. [72] for Cr^{3+} substituted samples, where $Li_3V_{1.59}Cr_{0.05}(PO_4)_3$@C and $Li_3V_{1.9}Cr_{0.1}(PO_4)_3$@C exhibited a by far better performance than unsubstituted LVP of (135 / 140 mAh/g) at 1 C, (120 / 130 mAh/g) at

3 C and (110 / 115 mAh/g) at 5 C for $Li_3V_{1.59}Cr_{0.05}(PO_4)_3$@C and $Li_3V_{1.9}Cr_{0.1}(PO_4)_3$@C in the potential range of 3.0 – 4.8 V vs. Li/Li respectively. In other words, the diffusion-controlled processes at 0.1 C are not directly comparable to the charge transfer kinetic or conductivity-controlled losses at 5 C.

Substitution with Mg=0.016 in LVP is considered as a good approach between delivered discharge capacity and coulombic efficiency as it shows close capacity values to the parent material and a close overall coulombic efficiency.

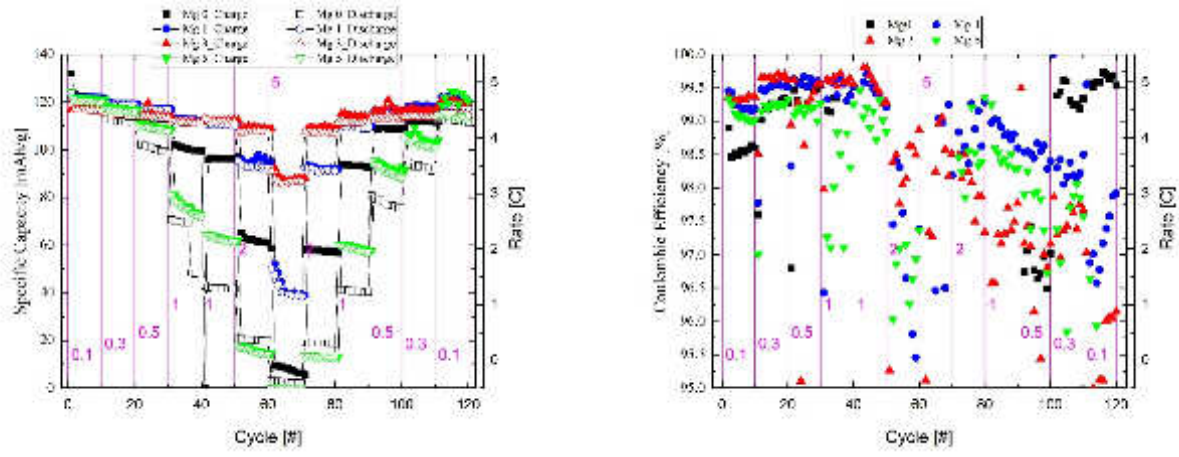

(a) (b)

Figure 5.1-VII Rate Capability (a) and Coulombic Efficiency (b) of LVP materials with different substitution concentrations in the potential range of 3.0 – 4.4 V vs. Li/Li⁺ - with the C-rates of C/10, C/3, C/2, 1C, 2C, 5C

5.1.5. Lithium diffusion coefficient

The calculations were started for the reactions $Li_3V_2(PO_4)_3$ to $Li_{2.5}V_2(PO_4)_3$ (at ~3.6 V) and $Li_{2.5}V_2(PO_4)_3$ to $Li_2V_2(PO_4)_3$ (at ~3.7 V) and compared for the different substitution concentrations. The measurements as well as mean values are shown in Table 5.1-II. It is worth mentioning that for σ_w correlations above 99.2 % have been found. For the samples containing Mg, $\frac{\partial E}{\partial x}$ for the first extraction was around 0.057 and the second 0.17. For the unsubstituted it was 0.12 for the first peak and 0.09 for the second. Nearly all results are within the same order of magnitude. Therefore, it is assumed that the method is valid. This leads to the conclusion that carbon coating has a greater influence than Mg on LVP in respect of apparent diffusion. Considering the unintended variations of the weight content of carbon (due to ambiguities of preparation) and the probably small influence of variation due to magnesium content it is obvious, that the carbon influence masks any effect. For research on the influence of magnesium on the diffusion coefficient samples with the same amount of in-situ carbon must be prepared, then the influence might be observed. The mentioned issue led to a stop in the investigation of this effect.

Comparing to Figure 5.1-V it can be seen, that at small C-rates the materials with high diffusivity (Mg0, Mg5) exhibit better capacity whereas at high C-rates Mg1 and Mg3 do.

Table 5.1-II Lithium Diffusion coefficients of LVP materials with different substitution concentrations

sample	D_{Li+} [cm²/s]	
	Li_3 -> $Li_{2.5}$	$Li_{2.5}$ -> Li_2
Mg0	$1.442*10^{-12}$	$4.903*10^{-12}$
Mg1	$7.416*10^{-12}$	$3.289*10^{-12}$
Mg3	$3.833*10^{-12}$	$2.542*10^{-12}$
Mg5	$2.804*10^{-11}$	$5.804*10^{-12}$

5.2. Electrochemical Results for the three Li^+-ion Transfer Cathode Material (3 – 4.9 V vs. Li/Li^+)

5.2.1. CV for different MG-substitution Concentrations

In Figure 5.2-I the first cycle of the CV measurement in the potential range of 3.0 - 4.9 V vs. Li/Li^+ for each substitution concentration is shown. The additional peak at 4.6 V vs. Li/Li^+ corresponds to the extraction of the third Li. This peak remains constant for different substitutions. Whereas the other peaks corresponding to the 1st Li+ extraction (~3.6 V vs. Li/Li^+) and 2nd Li^+ extraction (~4.1 V vs. Li/Li^+) tend to differ. Clearly visible is the two-phase region for reinsertion of lithium between 4.25 and 3.6 V. Moreover, only for the Mg1 sample the two-step insertions from Li_2 to Li_3 is visible as not a broad band, but as two independent sharp peaks. For Mg0 and Mg3 inconsistencies during the measurements occurred during insertion resulting in a tattered line. As previously mentioned each manufactured cell is different thus resulting in small variations of the reaction potential.

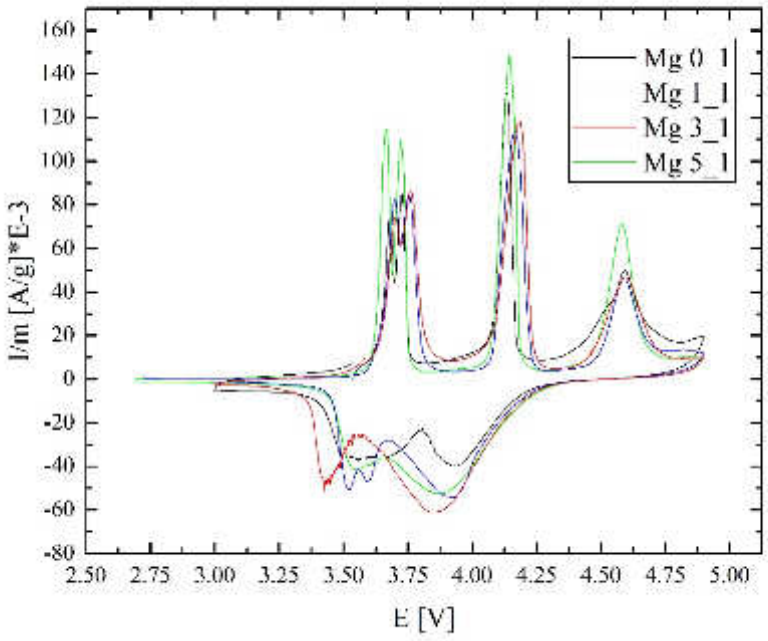

Figure 5.2-I Cyclic Voltammograms of LVP materials with different Mg-substitutions for the first cycle in the potential range of 3.0 – 4.9 V vs. Li/Li^+

In Figure 5.2-II, cyclic voltammograms of the Mg1 sample in the potential range of 3.0 - 4.9 V vs. Li/Li^+ are shown. Obviously, the peak height decreases from first to second cycle which is a sign of decreasing Li electroactivity. Also, small shifts of the peaks can be observed. Some of them would improve the energy efficiency. Charging peaks below 4.3 V shift to lower values while discharge peaks shift to higher voltages or stay the same (3.9 V). In contrast, the charging peak at high voltage first shifts to lower voltage and then to an even higher voltage. This means less energy efficiency for the overall process. In addition, the increasing overpotential between insertion and extraction voltages with cycle numbers indicates that the internal resistance is becoming higher and higher during cycling.

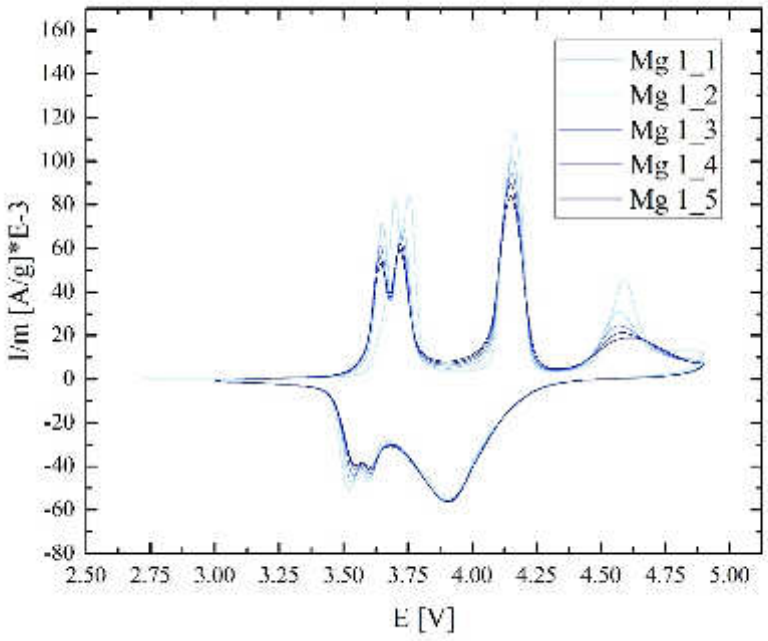

Figure 5.2-II Cyclic Voltammograms of Mg1 sample for five cycles in the potential range of 3.0 – 4.9 V vs. Li/Li⁺

5.2.2. Galvanostatic Cycling at C/10

The reason why LVP has been moved into focus of research is its high theoretical capacity of above 196 mAh/g for the full extraction process. Figure 5.2-III (a) and (b) display the long cycling performance for LVP materials with different substitution concentrations with C/10 in the potential range of 3.0 – 4.85 V vs. Li/Li⁺. The specific discharge capacity for different cycles are compared in Table 5.2-I. Mg5 with the highest initial discharge capacity of 155.45 mAh/g shows only 78 % of the theoretical value. Mg1 with the lowest initial capacity depicts around 75 %. After 10 cycles, the decrease of the specific capacity are 1.8 %, 3.6 %, 4.3 % and 7.5 % for Mg1, Mg5, Mg3 and Mg0, respectively. The high discharge capacity loss within the first ten cycles of the undoped material was also found for the cathodic two Li^+ ion process. Contrary to, for the smaller potential window a very small decrease is measured for the following 90 cycles. Whereas the capacity retention was above 97 % for the potential windows of 3 - 4.4 V vs. Li/Li⁺ and 80 – 83 % for the potential windows of 3 – 4.9 V vs. Li/Li⁺. Upon cycling the capacity fading can be seen for all samples. After 100 cycles Mg3 exhibits the highest discharge capacity of 122.4 mAh/g with the capacity retention of 83.6 %. The discharge capacity after 100 cycles is slightly higher in comparison to the two lithium exchange processes – except for the unsubstituted sample Mg0. The unsubstituted material exhibits a capacity of 111.9 mAh/g which is even lower than for the two Li^+-ion processes. As already previously mentioned is the inexplicable variational increase in charge capacity. Especially for Mg0 and Mg5 at the 40th and 82nd cycle respectively increased

charging capacity was observed while discharging capacity continuously faded. What can be said is that with increasing Mg content the stability enhances.

The decreasing stability and therefore capacity loss can have many causes. One of those is the structural stability of LVP. To conclude Mg substitution has shown to improve the structural stability of LVP, thus decrease the capacity losses in the potential range of 3 – 4.9 V vs. Li/Li^+. The poor electrochemical performance of the prepared materials can be attributed to the low stability of the LVP structures [19] and the electrolyte decomposition in the high-voltage region [73].

Table 5.2-I specific discharge capacitites for 3-4.9 V

electrode	discharge capacity at 1st cycle [mAh/g]	discharge capacity at 10th cycle [mAh/g]	discharge capacity at 50th cycle [mAh/g]	discharge capacity at 100th cycle [mAh/g]	capacity retention between 10th and 100th cycle [%]
Mg0	147.86	136.80	119.93	111.90	81.8
Mg1	146.74	144.09	128.45	119.45	82.9
Mg3	153.02	146.39	132.05	122.40	83.6
Mg5	155.45	149.86	128.70	120.00	80.1

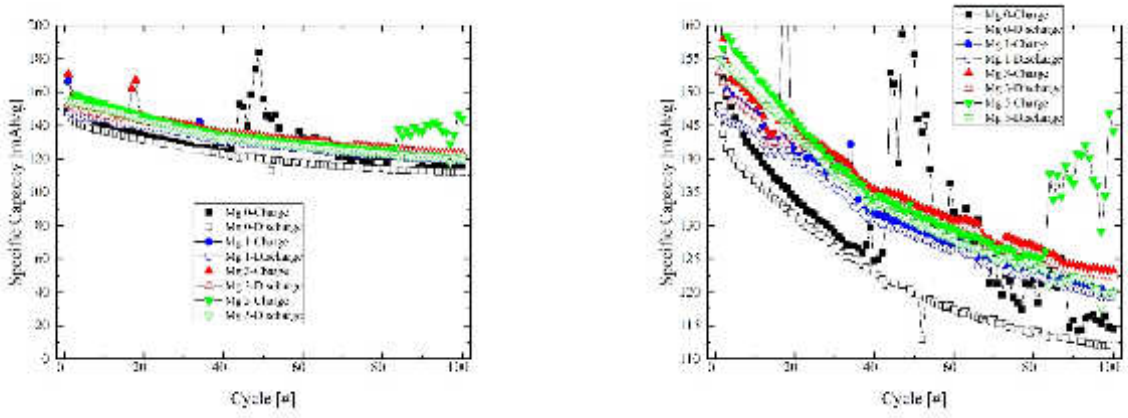

(a) (b)

Figure 5.2-III Specific capacity vs. cycle number for all substitution concentrations (3-4.9 V)

5.2.3. Coulombic Efficiency (CE)

The coulombic efficiency profiles are shown in Figure 5.2-IV (a) and (b). The initial coulombic efficiency lies around 90 %. A trend can be observed for all samples as they increase towards 100 % whereas only the samples with Mg substitution exceed 99 % after around 30 to 35 cycles. Whereas, the Mg0 shows stability problems as previously occurred. Mg1 demonstrated the best

performance with the coulombic efficiency of 99.5 % after 100 cycles compared to Mg5 and Mg3 with 99.2 % and 99.3 % respectively.

This effect of electrolyte stability and therefore electrolyte decomposition in the potential range of 3.0 – 4.9 V vs. Li/Li^+ were not independently examined. The commercial electrolyte 1 M LiPF6 in EC: DMC (1:1 by w/w) (LP30) is used as a stable electrolyte in the potential range of 0.8 – 4.4 V vs. Li/Li^+. [74]

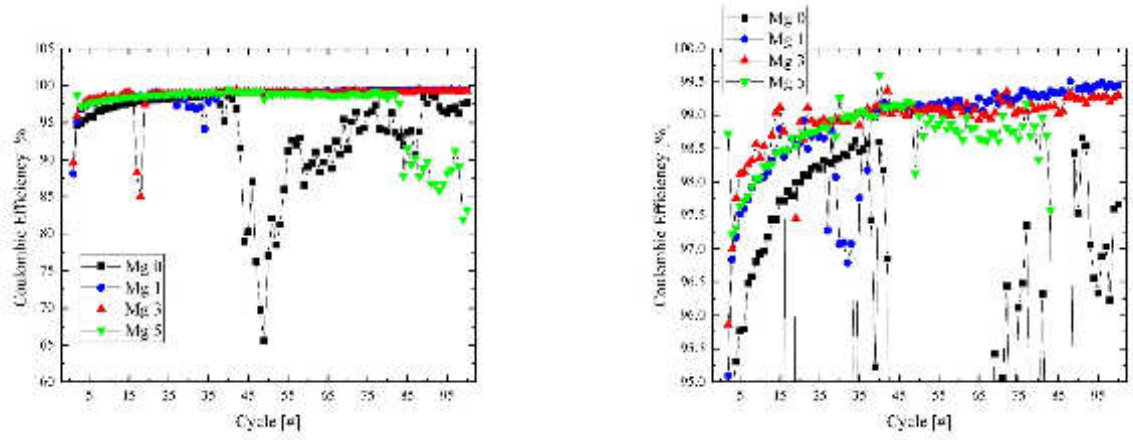

(a) (b)

Figure 5.2-IV Coulombic efficiency vs. cycle number for all substitution concentrations (3—4.8V)

5.2.4. Rate Capability

Figure 5.2-V (a) shows the specific capacity results from the rate capability test of LVP materials with different Mg substitution concentrations in the potential range of 3.0 – 4.9 V vs. Li/Li^+ with the C-rate of C/10, C/3, C/2, 1C, 2C and 5C. After 30 cycles at 1C, the degradation is clearly evident for Mg0 material (discharge capacity of ~50 mAh/g) which was also observed in the rate capability test in the potential window of 3.0 - 4.4 v vs. Li/Li^+ (Figure 5.1-VII). While Mg1 and Mg3 exhibit nearly no difference at 2C with the specific capacity of 105 mAh/g, Mg5 reveals a significant drop to around 45 mAh/g. This trend prolongs for higher C.rates. At 5C Mg0 exhibits no capacity due to instability in the structure which cause it to collapse. The reason that Mg5 exhibits no capacity at 5C is due to the missing in-situ carbon coating.

Coulombic efficiency profiles for the rate capability test are shown in Figure 5.2-V (b). The irrational CE values derived at high C-rates for the capacities around 0 mAh/g as well as CE values around rate changes were excluded from the graph. The CE around 99 % could be achieved after 20 cycles for the substituted samples, whereas drastic losses at high C-rates (>1C) are shown for the unsubstituted sample.

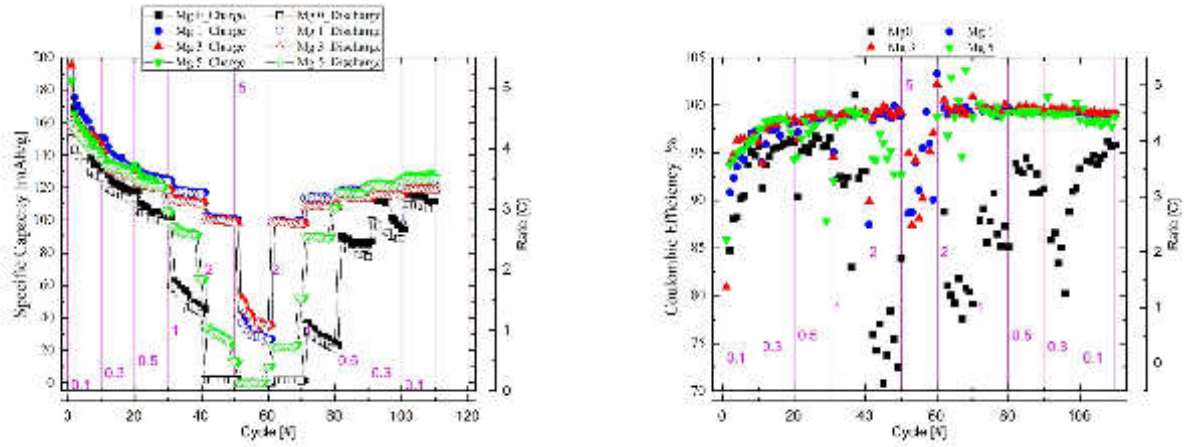

(a) (b)

Figure 5.2-V Rate Capability (a) and Coulombic Efficiency (b) of LVP materials with different substitution concentrations in the potential range of 3.0 – 4.9 V vs. Li/Li⁺ - with the C-rates of C/10, C/3, C/2, 1C, 2C, 5C

5.3. Electrochemical Results for Two Li^+-ion Transfer Anode Material (1.0 – 2.4 V vs. Li/Li^+)

5.3.1. CV for different Mg-substitution concentrations

Anode cycling between 2.4 and 1.0 V vs. Li/Li^+ is interesting because the measure OCV of the manufactured cells is around 3- 3.4 V. Figure 3.3-IV shows the cyclic voltammograms for different no reactions occur during 3.5 and ~2 V. Mao et.al. [75] proposes a four step (each 0.5 Li^+) mechanism for the anodic reactions. The insertion (charge) part of this mechanism can be seen in Figure 5.3-I. at for example Mg5 and the unsubstituted Mg0. For the discharge process a shoulder and broadening of the first peak can be observed instead of four separate peaks. For Mg1 and Mg3 more vague results are obtained.

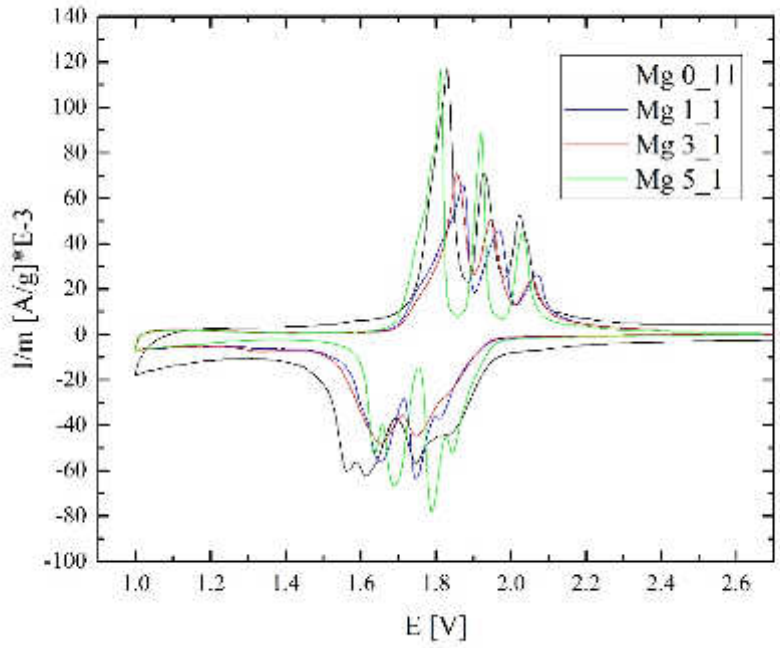

Figure 5.3-I Cyclic Voltammograms of LVP materials with different Mg substitution for the first cycle in the potential range of 1.0 - 2.4 V vs. Li/Li^+

Figure 5.3-II shows the first 6 cycles of anodic cycling of Mg5. For graphite as an anode material a drastic capacity loss (up to one third of the capacity) is observed for the first cycles, because the SEI (solid electrolyte interface) is formed. Such an effect is not witnessed for LVP. Only little degradation processes during insertion occur and peak broadening can be observed. Below 1.4 V no reactions are observed.

Experiments regarding further lithiation to $Li_7V_2(PO_4)_3$ in the potential range 2.4 – 0.4 V vs. Li/Li^+ were not enlightening as the electrolyte stability (0.8 – 4.4 V) spoiled the desired experiments.

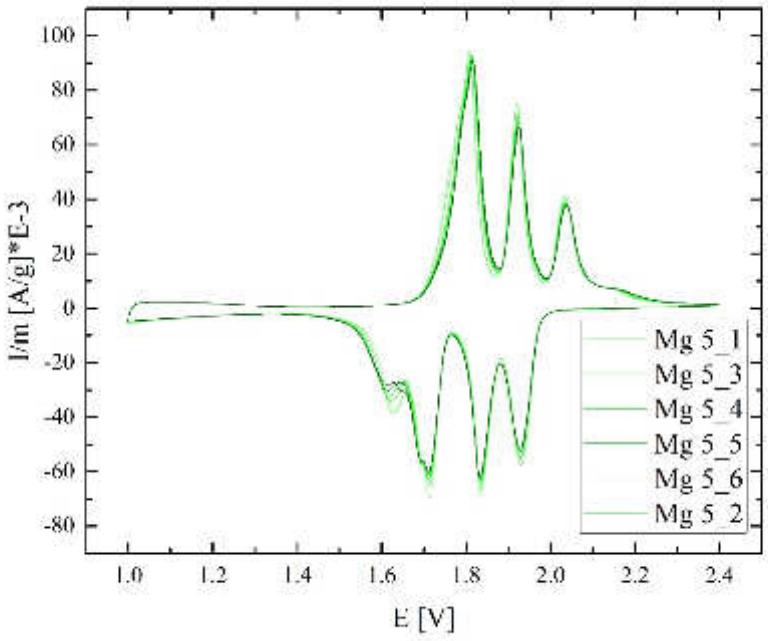

Figure 5.3-II Cyclic Voltammograms of the sample Mg5 for the first 6 cycles in the potential range of 1.0-2.4 V vs. Li/Li⁺

5.3.2. Galvanostatic Cycling at C/10

The measured initial capacities of the LVP@C are around 94 % of the theoretically achievable. Mg3 exhibits the lowest initial capacity whereas the capacity retention over 100 cycles is the best. Most materials exhibit a steep decrease of around 5 % (7 mAh/g) within the first ten cycles except Mg5 (only 1.5 %). The capacity retention between the 10th and the 100th cycle is approximately the same for all materials. Mg1 exhibits worse properties. This can be due to preparation of the electrode, because from optical assessment the coated foil seemed different in color and consistency. This would explain the high drop-out rate of the manufactured cells of around 70 % as well as the bad results obtained during cycling. In comparison to the galvanostatic cycling shown in 5.3, where the degradation of the cells seemed drastically accelerated. An interesting aspect is the comparable capacity of the undoped material leading to the conclusion that magnesium does not influence the anodic properties. From theoretical considerations magnesium should stabilize the crystal structure during full delithiation and shortage of the V-O bonds. For the negative electrode this is not necessary (as in 2.3.4 mentioned), because during charging additional lithium is inserted into the system, concluding there is no need for stabilization. Nevertheless, different capacities were observed for the differently substituted materials. The highest capacity was measured with the Mg5 sample as shown in Table 5.3-I. The steadiest capacity is observed at Mg3 where the capacity retention from 10th to 100th is above 95 %.

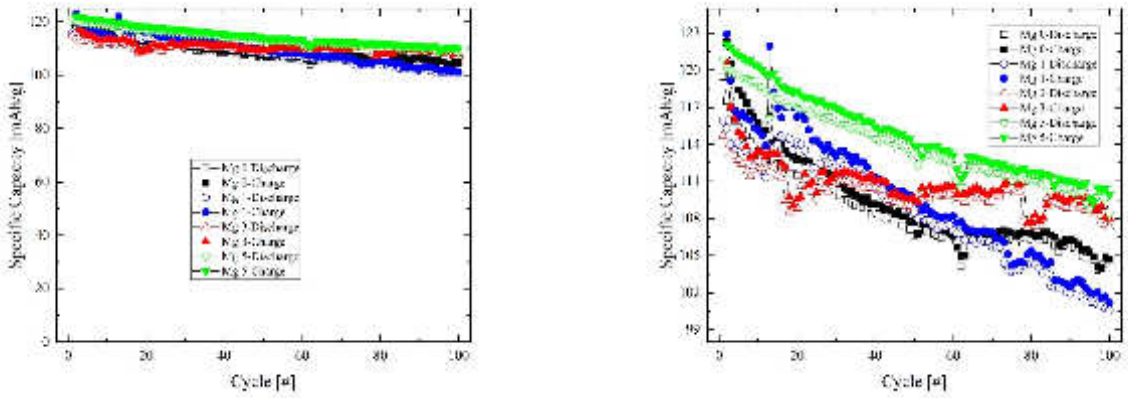

(a) (b)

Figure 5.3-III Specific capacity vs. cycle number for LVP materials with different substitution concentrations with C/10 in the potential range of 2.4 – 1.0 V vs. Li/Li⁺ (a) and zoomed to 99 – 125 mAh/g (b)

Table 5.3-I Specific discharge capacities at 1-10-50-100 cycles of GC

electrode	discharge capacity at 1st cycle [mAh/g]	discharge capacity at 10th cycle [mAh/g]	discharge capacity at 50th cycle [mAh/g]	discharge capacity at 100th cycle [mAh/g]	capacity retention between 10th and 100th cycle [%]
Mg0	122.23	115.74	107.70	104.70	90.5
Mg1	122.92	115.12	109.24	101.20	87.9
Mg3	120.57	113.43	109.61	108.03	95.2
Mg5	122.08	120.35	113.91	109.93	91.3

5.3.3. Coulombic Efficiency (CE)

The data for CE is displayed in Figure 5.3-IV (a) and (b). All samples exhibit superior CE and after 15 cycles all samples have reached coulombic efficiencies above 99 % independently if the samples are substituted or not. Sometimes CEs higher than 100 % can be observed. They are explicable by delayed release of stored Li^+. This effect mostly occurs directly after a decline. Mg1 exhibits the worse CE. The reason therefore lies as previously mentioned in the anode preparation. It is safe to say, that magnesium's influence on the electrochemical properties of LVP as an anode material are not significant even though two of the investigated materials exhibit higher capacities by 3 % and 4.8 % after 100 cycles for Mg3 and Mg5 respectively. The coulombic efficiency exhibits almost equal properties.

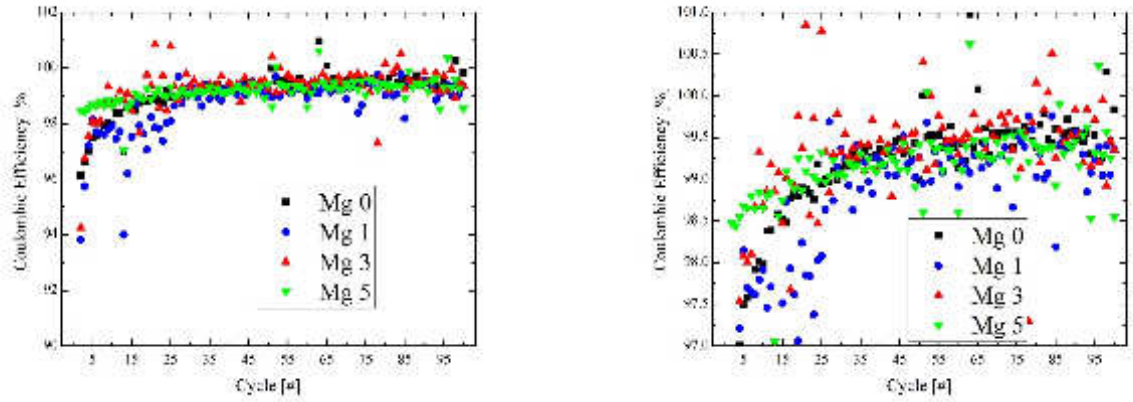

(a) (b)

Figure 5.3-IV Coulombic efficiency vs cycle number profiles for LVP materials with different substitution concentrations in the potential range of 1.0 - 2.4 V vs. Li/Li^+ (a); zoomed 97-101 % (b)

6 Conclusion

To summarize what this thesis has proven to be relevant for the initially posed question: "How does Mg-doping influence stability, particle size, capacity, coulombic efficiency and capacity retention of LVP as an electrode material?" the following points should be emphasized.

In this thesis, a series of $Li_3V_{(2-2x/3)}Mg_x(PO_4)_3$@C with x=0, 0.016, 0.037, 0.053 were synthesized through combustion sol-gel method with consequent annealing at 750°C under argon. To improve the electronic conductivity and Li+-ion diffusivity, carbon coating was performed by milling with dissolved sucrose as well as addition of amorphous carbon in the cells. XRD patterns show that Mg^{2+} successfully substituted small amounts of V^{3+} in the structure of $Li_3V_2(PO_4)_3$ with monoclinic $P2_1/c$ symmetry without impurities. SEM images showed similar morphology for all materials. EDX revealed homogenous distribution of O, P, V. Based on the N_2 adsorption/ desorption analyses, materials revealed that all synthesized materials exhibit mesoporous properties with the pore size ranging 9 to 18 nm and specific surface area of 24 to 85 m² with small pores and big surface area for the unsubstituted sample. The materials have a particle size smaller than 1 µm for the substituted samples which tend to agglomerate, while the one without magnesium exhibits a particle size around 4-5 µm.

Cyclic voltammetry measurements confirm that Mg^{2+} is electrochemically inactive in the potential range of 3.0 – 4.9 V vs. Li/Li^+. Mg substitution has been shown to enhance the structure stability at high C-rates. Substitution with x= 0.037 in LVP@C can be considered as a good compromise between delivered discharge capacity and coulombic efficiency as a cathode material. The material exhibits a capacity of 87 mAh/g at 5 C in the potential range of 3.0 - 4.4 V and of 95 mAh/g at 5Cin the range of 3.0 – 4.9 V vs. Li/Li^+ as well as the highest capacity retention 84 % (10^{th} to 100^{th} cycle) in the range of 3.0 – 4.9 V vs. Li/Li^+.

In the high-potential window the LVP materials show a rapid capacity fading which can be attributed to the low stability of the LVP crystal structures and the electrolyte decomposition in the high-voltage region. Magnesium significantly increases the actually available discharge capacities in both potential regions.

Effective and homogeneous carbon coating is of great importance for high current application as it improves the electronic conductivity and facilitates the Li^+-ion diffusion.

Hence the development of synthetic routes to achieve optimized carbon-coated / cation-substituted composite LVP nanoparticles with high stability in the high voltage remains necessary.

Future work should focus on testing negative electrode properties for higher C-rates and a wider potential window up to of $Li_7V_2(PO_4)_3$.

7 Abbreviations

abbreviation	description
AM	active material
AMCct	active material carbon coated
BET	Brunauer-Emmet-Teller – scientist who invented a method to calculate surface area and pore size via adsorption / desorption processes of N_2 on the sample's surface
CCCV	charging mode: constant current constant voltage
CE	coulombic efficiency
CM	conductive material
CV	cyclic voltammetry
DTA	differential thermal analysis
EDX	energy dispersive x-ray spectroscopy
EIS	electrochemical impedance spectroscopy
EV	electric vehicle
GC	galvanostatic cycling
HEV	hybrid electric vehicle
ICP-OES	ion coupled plasma optical emission spectroscopy
LIB	lithium ion battery
LP30	electrolyte consisting of 1 M $LiPF_6$ in EC: DMC = 1:1 w/w
LSV	linear sweep voltammetry
LVP	$Li_3V_{(2-2x/3)}Mg_x(PO_4)_3$ this thesis' central substance
LVP@C	carbon coated LVP
NMP	n-methylpyrrolidone
OCV	open circuit voltage – cell voltage of a pristine cell [V]
PEIS	potentiostatic electrochemical impedance spectroscopy
PVDF	polyvinylidendiflourid
RC	rate capability
SEM	secondary electron microscopy
TG	thermogravimetry
XRD	x-ray diffraction spectroscopy
YSZ	yttria stabilized zirconiumoxide

8 References

[1] K. Nagura, T. Tozawa, "Lithium ion rechargable battery," *Prog. Batter. Sol. Cells*, no. 9, p. 209, 1990.

[2] "full cell: lithiumferrophosphate | graphite," 2014. [Online]. Available: http://pubs.rsc.org/services/images/RSCpubs.ePlatform.Service.FreeContent.ImageService.svc/ImageService/Articleimage/2014/EE/c4ee01432d/c4ee01432d-f1_hi-res.gif. [Accessed: 28-Apr-2018].

[3] M. S. Whittingham, "Lithium batteries and cathode materials," *Chem. Rev.*, vol. 104, no. 10, pp. 4271–4301, 2004.

[4] J. B. Goodenough and Y. Kim, "Challenges for rechargeable Li batteries," *Chem. Mater.*, vol. 22, no. 3, pp. 587–603, 2010.

[5] T. Ohzuku, "Electrochemistry and Structural Chemistry of LiNiO[sub 2] (R3m) for 4 Volt Secondary Lithium Cells," *J. Electrochem. Soc.*, vol. 140, no. 7, p. 1862, 1993.

[6] J. Cho, Y.-W. Kim, B. Kim, J.-G. Lee, and B. Park, "A Breakthrough in the Safety of Lithium Secondary Batteries by Coating the Cathode Material with AlPO4 Nanoparticles," *Angew. Chemie Int. Ed.*, vol. 42, no. 14, pp. 1618–1621, Apr. 2003.

[7] J. Sakurai, Yoji (Mito, J. Hirai, Toshiro (Mito, J. Okada, Shigeto (Mito, J. Okada, Takeshi (Mito, J. Yamaki, Jun-ichi (Mito, and J. Ohtsuka, Hideaki (Mito, "Lithium battery including vanadium pentoxide base amorphous cathode active material," 1991.

[8] Z. Liu, A. Yu, and J. Y. Lee, "..," *Power Sources*, no. 416, pp. 81–82, 1999.

[9] M. Yoshio, H. Noguchi, J. ichi Itoh, M. Okada, and T. Mouri, "Preparation and properties of LiCoyMnxNi1-x-yO2 as a cathode for lithium ion batteries," *J. Power Sources*, vol. 90, no. 2, pp. 176–181, 2000.

[10] T. Ohzuku and Y. Makimura, "Layered Lithium Insertion Material of LiCo 1/3 Ni 1/3 Mn 1/3 O 2 for Lithium-Ion Batteries," *Chem. Lett.*, vol. 30, no. 7, pp. 642–643, 2001.

[11] J. K. Ngala, N. A. Chernova, M. Ma, M. Mamak, P. Y. Zavalij, and M. S. Whittingham, "The synthesis , characterization and electrochemical behavior of the layered LiNi 0 . 4 Mn 0 . 4 Co 0 . 2 O 2 compound," no. Li, 2004.

[12] B. J. Hwang, Y. W. Tsai, D. Carlier, and G. Ceder, "A combined computational/experimental study on LiNi1/3Co 1/3Mn1/3O2," *Chem. Mater.*, vol. 15, no. 19, pp. 3676–3682, 2003.

[13] I. Saadoune and C. Delmas, "LiNi 1–y Co y O 2 positive electrode materials: relationships between the structure, physical properties and electrochemical behaviour," *J. Mater. Chem.*, vol. 6, no. 2, pp. 193–199, 1996.

[14] S. W. Oh, S. H. Park, C. W. Park, and Y. K. Sun, "Structural and electrochemical properties of layered Li[Ni0.5Mn0.5]1-xCoxO2positive materials synthesized by ultrasonic spray pyrolysis method," *Solid State Ionics*, vol. 171, no. 3–4, pp. 167–172, 2004.

[15] Y. Sun, C. Ouyang, Z. Wang, X. Huang, and L. Chen, "Effect of Co Content on Rate Performance of LiMn[sub 0.5–x]Co[sub 2x]Ni[sub 0.5–x]O[sub 2] Cathode Materials for Lithium-Ion Batteries," *J. Electrochem. Soc.*, vol. 151, no. 4, p. A504, 2004.

[16] X. H. Rui, Y. Jin, X. Y. Feng, L. C. Zhang, and C. H. Chen, "A comparative study on the low-temperature performance of LiFePO4/C and Li3V2(PO4)3/C cathodes for lithium-ion batteries," *J. Power Sources*, vol. 196, no. 4, pp. 2109–2114, 2011.

[17] A. Yamada, S. C. Chung, and K. Hinokuma, "Optimized LiFePO[sub 4] for Lithium Battery Cathodes," *J. Electrochem. Soc.*, vol. 148, no. 3, p. A224, 2001.

[18] N. N. Bramnik, K. Nikolowski, G. Baehtz, K. G. Bramnik, and H. Ehrenberg, "Phase transitions occurring upon lithium insertion-extraction of LiCoPO4," *Chem. Mater.*, vol. 19, no. 4, pp. 908–915, 2007.

[19] L. Wang, J. Xu, C. Wang, X. Cui, J. Li, and Y.-N. Zhou, "A better understanding of the capacity fading mechanisms of $Li_3V_2(PO_4)_3$," *RSC Adv.*, vol. 5, no. 88, pp. 71684–71691, 2015.

[20] F. Zhou, M. Cococcioni, K. Kang, and G. Ceder, "The Li intercalation potential of LiMPO4 and LiMSiO4 olivines with M=Fe, Mn, Co, Ni," *Electrochem. Community*, vol. 6, pp. 1144–1148, 2004.

[21] A. K. Padhi, K. S. Nanjundaswamy, and J. B. Goodenough, "Phospho-olivines as Positive-Electride Materials for Rechargeable Lithium Batteries," *J. Electrochem. Soc.*, vol. 144, no. 4, pp. 1188–1194, 1997.

[22] Z. Chen and J. R. Dahn, "Reducing Carbon in LiFePO[sub 4]/C Composite Electrodes to Maximize Specific Energy, Volumetric Energy, and Tap Density," *J. Electrochem. Soc.*, vol. 149, no. 9, p. A1184, 2002.

[23] J. Shim and K. A. Striebel, "Cycling performance of low-cost lithium ion batteries with natural graphite and LiFePO4," *J. Power Sources*, vol. 119–121, pp. 955–958, 2003.

[24] M. Y. Saidi, J. Barker, H. Huang, J. L. Swoyer, and G. Adamson, "Electrochemical properties of lithium vanadium phosphate as a cathode material for lithium-ion batteries," *Electrochem. Solid State Lett.*, vol. 5, no. 7, pp. A149–A151, 2002.

[25] A. K. Padhi, "Mapping of Transition Metal Redox Energies in Phosphates with NASICON Structure by Lithium Intercalation," *J. Electrochem. Soc.*, vol. 144, no. 8, p. 2581, 1997.

[26] J. Gaubicher, C. Wurm, G. Goward, C. Masquelier, and L. Nazar, "Rhombohedral form of Li3V2(PO4)3 as a cathode in Li-ion batteries," *Chem. Mater.*, vol. 12, no. 11, pp. 3240–3242, 2000.

[27] S. C. Yin, H. Grondey, P. Strobel, M. Anne, and L. F. Nazar, "Electrochemical property: Structure relationships in monoclinic Li3-yV2(PO4)3," *J. Am. Chem. Soc.*, vol. 125, no. 34, pp. 10402–10411, 2003.

[28] M. Y. Saïdi, J. Barker, H. Huang, J. L. Swoyer, and G. Adamson, "Performance characteristics of lithium vanadium phosphate as a cathode material for lithium-ion batteries," *J. Power Sources*, vol. 119–121, pp. 266–272, 2003.

[29] S.-W. Choi, D.-H. Kim, S.-H. Yang, M.-Y. Kim, M.-S. Lee, and H.-S. Kim, "The studies of lattice parameter and electrochemical behavior for Li3V2(PO4)3/C cathode materials," *J. Ind. Eng. Chem.*, vol. 52, pp. 314–320, Aug. 2017.

[30] H. Huang, S. C. Yin, T. Kerr, N. Taylor, and L. F. Nazar, "Nanostructured composites: A high capacity, fast rate Li3V2(PO4)3/carbon cathode for rechargeable lithium batteries," *Adv. Mater.*, vol. 14, no. 21, pp. 1525–1528, 2002.

[31] X. Rui, Q. Yan, M. Skyllas-Kazacos, and T. M. Lim, "Li3V2(PO4)3cathode materials for lithium-ion batteries: A review," *J. Power Sources*, vol. 258, pp. 19–38, 2014.

[32] S. Patoux, C. Wurm, M. Morcrette, G. Rousse, and C. Masquelier, "A comparative structural and electrochemical study of monoclinic Li3Fe2(PO4)3and Li3V2(PO4)3," *J. Power Sources*, vol. 119–121, pp. 278–284, 2003.

[33] X. H. Rui, N. Ding, J. Liu, C. Li, and C. H. Chen, "Analysis of the chemical diffusion coefficient of lithium ions in Li3V2(PO4)3cathode material," *Electrochim. Acta*, vol. 55, no. 7, pp. 2384–2390, 2010.

[34] X. H. Rui, N. Yesibolati, and C. H. Chen, "Li3V2(PO4)3/C composite as an intercalation-type anode material for lithium-ion batteries," *J. Power Sources*, vol. 196, no. 4, pp. 2279–2282, 2011.

[35] H. Liu *et al.*, "Kinetics of conventional carbon coated-Li3V2(PO4)3 and nanocomposite Li3V2(PO4)3/graphene as cathode materials for lithium ion batteries," *J. Mater. Chem.*, vol. 22, no. 22, p. 11039, 2012.

[36] J. Molenda, A. Stokłosa, and T. Bąk, "Modification in the electronic structure of cobalt bronze LixCoO2and the resulting electrochemical properties," *Solid State Ionics*, vol. 36, no. 1–2, pp. 53–58, 1989.

[37] M. Nishizawa, T. Ise, H. Koshika, T. Itoh, and I. Uchida, "Electrochemical in-situ conductivity measurements for thin film of Li(1-x)Mn2O4spinel," *Chem. Mater.*, vol. 12, no. 5, pp. 1367–1371, 2000.

[38] P. Fu, Y. Zhao, Y. Dong, X. An, and G. Shen, "Low temperature solid-state synthesis routine and mechanism for Li 3 V 2 (PO 4) 3 using LiF as lithium precursor," vol. 52, pp. 1003–1008, 2006.

[39] Z. Chen *et al.*, "High performance Li3V2(PO4)3/C composite cathode material for lithium ion batteries studied in pilot scale test," *Electrochim. Acta*, vol. 55, no. 28, pp. 8595–8599, 2010.

[40] G. Yang, H. Ji, H. Liu, B. Qian, and X. Jiang, "Electrochimica Acta Crystal structure and electrochemical performance of Li 3 V 2 (PO 4) 3 synthesized by optimized microwave solid-state synthesis route," *Electrochim. Acta*, vol. 55, no. 11, pp. 3669–3680, 2010.

[41] L. Zhang, H. Xiang, Z. Li, and H. Wang, "Porous Li3V2(PO4)3/C cathode with extremely high-rate capacity prepared by a sol-gel-combustion method for fast charging and discharging," *J. Power Sources*, vol. 203, no. 3, pp. 121–125, 2012.

[42] X. J. Zhu, Y. X. Liu, L. M. Geng, and L. B. Chen, "Synthesis and performance of lithium vanadium phosphate as cathode materials for lithium ion batteries by a sol-gel method," *J. Power Sources*, vol. 184, no. 2, pp. 578–582, 2008.

[43] X. H. Rui, C. Li, J. Liu, T. Cheng, and C. H. Chen, "Electrochimica Acta The Li 3 V 2 (PO 4) 3 / C composites with high-rate capability prepared by a maltose-based sol – gel route," vol. 55, pp. 6761–6767, 2010.

[44] Y. Li, Z. Zhou, M. Ren, X. Gao, and J. Yan, "Electrochemical performance of nanocrystalline Li 3 V 2 (PO 4) 3 / carbon composite material synthesized by a novel sol – gel method," vol. 51, pp. 6498–6502, 2006.

[45] W. Duan, Z. Hu, K. Zhang, F. Cheng, Z. Tao, and J. Chen, "Li3V2(PO4)3@C core–shell nanocomposite as a superior cathode material for lithium-ion batteries," *Nanoscale*, vol. 5, no. 14, p. 6485, 2013.

[46] X. H. Rui, C. Li, and C. H. Chen, "Electrochimica Acta Synthesis and characterization of carbon-coated Li 3 V 2 (PO 4) 3 cathode materials with different carbon sources," vol. 54, pp. 3374–3380, 2009.

[47] T. Jiang, C. Wang, G. Chen, H. Chen, Y. Wei, and X. Li, "Effects of synthetic route on the structural , physical and electrochemical properties of Li 3 V 2 (PO 4) 3 cathode materials," *Solid State Ionics*, vol. 180, no. 9–10, pp. 708–714, 2009.

[48] K. Nathiya, D. Bhuvaneswari, Gangulibabu, D. Nirmala, and N. Kalaiselvi, "Li3MxV2–x(PO4)3/C (M=Fe, Co) composite cathodes with extended solubility limit and improved electrochemical behavior," *RSC Adv.*, vol. 2, no. 17, p. 6885, 2012.

[49] M. Ren, Z. Zhou, Y. Li, X. P. Gao, and J. Yan, "Preparation and electrochemical studies of Fe-doped Li3V2(PO4)3cathode materials for lithium-ion batteries," *J. Power Sources*, vol. 162, no. 2 SPEC. ISS., pp. 1357–1362, 2006.

[50] Q. Kuang, Y. Zhao, X. An, J. Liu, Y. Dong, and L. Chen, "Synthesis and electrochemical properties of Co-doped Li3V2(PO4)3cathode materials for lithium-ion batteries," *Electrochim. Acta*, vol. 55, no. 5, pp. 1575–1581, 2010.

[51] J. Yao, S. Wei, P. Zhang, C. Shen, K. F. Aguey-Zinsou, and L. Wang, "Synthesis and properties of Li3V2-xCex(PO4)3/C cathode materials for Li-ion batteries," *J. Alloys Compd.*, vol. 532, pp. 49–54, 2012.

[52] M. Bini, S. Ferrari, D. Capsoni, and V. Massarotti, "Mn influence on the electrochemical behaviour of Li3V2(PO4)3 cathode material," *Electrochim. Acta*, vol. 56, no. 6, pp. 2648–2655, Feb. 2011.

[53] W. Wu, J. Liang, J. Yan, and W. Mao, "Synthesis of Li3Ni x V2–x (PO4)3/C cathode materials and their electrochemical performance for lithium ion batteries," *J. Solid State Electrochem.*, vol. 17, no. 7, pp. 2027–2033, 2013.

[54] D. Ai, K. Liu, Z. Lu, M. Zou, D. Zeng, and J. Ma, "Aluminothermal synthesis and characterization of Li3V 2-xAlx(PO4)3 cathode materials for lithium ion batteries," *Electrochim. Acta*, vol. 56, no. 7, pp. 2823–2827, 2011.

[55] J. Yao, S. Wei, P. Zhang, C. Shen, K.-F. Aguey-Zinsou, and L. Wang, "Synthesis and properties of Li3V2–xCex(PO4)3/C cathode materials for Li-ion batteries," *J. Alloys Compd.*, vol. 532, pp. 49–54, Aug. 2012.

[56] J. S. Huang, L. Yang, K. Y. Liu, and Y. F. Tang, "Synthesis and characterization of Li3V(2 - 2x/3)Mgx(PO4)3/C cathode material for lithium-ion batteries," *J. Power Sources*, vol. 195, no. 15, pp. 5013–5018, 2010.

[57] C. Dai, Z. Chen, H. Jin, and X. Hu, "Synthesis and performance of Li3(V1–xMgx)2(PO4)3 cathode materials," *J. Power Sources*, vol. 195, no. 17, pp. 5775–5779, Sep. 2010.

[58] C. Deng *et al.*, "Effects of Ti and Mg Codoping on the Electrochemical Performance of $Li_3V_2(PO_4)_3$ Cathode Material for Lithium Ion Batteries," *J. Phys. Chem. C*, vol. 115, no. 30, pp. 15048–15056, 2011.

[59] Wikibooks-Bearbeiter, "Bibliografische Angaben für Tabellensammlung Chemie/ Atom- und Ionenradien," *Wikibooks, Die freie Bibliothek*. [Online]. Available: https://de.wikibooks.org/w/index.php?title=Tabellensammlung_Chemie/_Atom-_und_Ionenradien&oldid=827500. [Accessed: 15-May-2018].

[60] Z. Chen, G. Yuan, C. Dai, X. Hu, and X. Luo, "Electrochemical behavior of Mg-doped 7LiFePO4-Li3V2(PO4)3 composite cathode material for lithium-ion batteries," *Ionics (Kiel).*, vol. 19, no. 8, pp. 1077–1084, 2013.

[61] B. Wunderlich, "Thermal Analysis," *Encycl. Mater. Sci. Technol.*, pp. 9134–9141, Jan. 2001.

[62] S. Brunauer, P. H. Emmett, and E. Teller, "Adsorption of Gases in Multimolecular Layers," *J. Am. Chem. Soc.*, vol. 60, no. 2, pp. 309–319, Feb. 1938.

[63] D. I. für Normung, *Determination of the specific surface area of solids by gas adsorption - BET method (ISO 9277:2010)*. 2014.

[64] J. Shin, J. Yang, C. Sergey, M. S. Song, and Y. M. Kang, "Carbon Nanofibers Heavy Laden with Li3V2(PO4)3Particles Featuring Superb Kinetics for High-Power Lithium Ion Battery," *Adv. Sci.*, vol. 4, no. 9, pp. 1–9, 2017.

[65] C. Ho, "Application of A-C Techniques to the Study of Lithium Diffusion in Tungsten Trioxide Thin Films," *J. Electrochem. Soc.*, vol. 127, no. 2, p. 343, 1980.

[66] C. Deng *et al.*, "Effects of Ti and Mg Codoping on the Electrochemical Performance of $Li_3V_2(PO_4)_3$ Cathode Material for Lithium Ion Batteries," *J. Phys. Chem. C*, vol. 115, no. 30, pp. 15048–15056, 2011.

[67] E. Kobayashi, A. Kitajou, S. Okada, and J. I. Yamaki, "Improvement of solid-state symmetric cell performance with lithium vanadium phosphate," *J. Power Sources*, vol. 244, pp. 312–317, 2013.

[68] S. Y. Yang, S. Zhang, B. L. Fu, Q. Wu, F. L. Liu, and C. Deng, "Effects of Cr doping on the electrochemical performance of Li3V2(PO4)3 cathode material for lithium ion batteries," *J. Solid State Electrochem.*, vol. 15, no. 11–12, pp. 2633–2638, 2011.

[69] A. Eftekhari and Z. Fan, "Ordered mesoporous carbon and its applications for electrochemical energy storage and conversion," *Mater. Chem. Front.*, vol. 1, no. 6, pp. 1001–1027, 2017.

[70] S.-C. Yin, H. Grondey, P. Strobel, M. Anne, and L. F. Nazar, "Electrochemical Property: Structure Relationships in Monoclinic Li3-yV2(PO4)3," *J. Am. Chem. Soc.*, vol. 125, no. 34, pp. 10402–10411, Aug. 2003.

[71] T. Seilnacht, "Basic Knowledge about Chemistry." Seilnacht Verlag & Atelier, Bern, 2018.

[72] Y. Chen, Y. Zhao, X. An, J. Liu, Y. Dong, and L. Chen, "Preparation and electrochemical performance studies on Cr-doped Li3V2(PO4)3as cathode materials for lithium-ion batteries," *Electrochim. Acta*, vol. 54, no. 24, pp. 5844–5850, 2009.

[73] J. Kasnatscheew, B. Streipert, S. Röser, R. Wagner, I. Cekic Laskovic, and M. Winter, "Determining oxidative stability of battery electrolytes: validity of common electrochemical stability window (ESW) data and alternative strategies," *Phys. Chem. Chem. Phys.*, vol. 19, no. 24, pp. 16078–16086, 2017.

[74] K. Frohlich, G. Bimashofer, G. Fafilek, F. Pichler, M. Cifrain, and A. Trifonova, "Electrochemical Investigation of Thermodynamic and Transport Phenomena in LP30 Electrolyte with Various Concentrations of Conducting Salt," *ECS Trans.*, vol. 73, no. 1, pp. 83–93, 2016.

[75] W. -f. Mao, H. -q. Tang, Z. -y. Tang, J. Yan, and Q. Xu, "Configuration of Li-Ion Vanadium Batteries: Li3V2(PO4)3(cathode) Li3V2(PO4)3(anode)," *ECS Electrochem. Lett.*, vol. 2, no. 7, pp. A69–A71, 2013.